Passive Seismic Characterization of High Priority Salt Jugs Near Hutchinson, Kansas: December 2019

Sarah L. Morton, Shelby Peterie, Julian Ivanov, Richard Miller, Brett Bennett, Cole Bunker, Kristen Burke, Erik Knippel, Jeff Lawler, Connor Umbrell, and Brett Wedel

Kansas Geological Survey
1930 Constant Avenue
Lawrence, KS 66047

Report to

Narayanan Raghupathi
Burns & McDonnell Engineering Company Inc.
1431 Opus Place, Suite 400
Downers Grove, IL 60615
630-724-3259

Open-file Report 2020-15 March 2020

The Kansas Geological Survey makes no warranty or representation, either express or implied, with regard to the data, documentation, or interpretations or decisions based on the use of this data including the quality, performance, merchantability, or fitness for a particular purpose. Under no circumstances shall the Kansas Geological Survey be liable for damages of any kind, including direct, indirect, special, incidental, punitive, or consequential damages in connection with or arising out of the existence, furnishing, failure to furnish, or use of or inability to use any of the database or documentation whether as a result of contract, negligence, strict liability, or otherwise. This study was conducted in complete compliance with ASTM Guide D7128-05. All data, interpretations, and opinions expressed or implied in this report and associated study are reasonably accurate and in accordance with generally accepted scientific standards.

Passive Seismic Characterization of High Priority Salt Jugs Near Hutchinson, Kansas: December 2019

Executive Summary

This applied research project appraised stress conditions of rock above dissolution voids by estimating the relative stress field from the shear-wave velocity of the overburden. Shear-wave velocities were calculated during this study using passive surface-wave methods. Data were acquired along two profiles located on or near key abandoned brine production wells using train traffic as an energy source. Multichannel analysis of surface waves (MASW) method was used to estimate the shear-wave velocity, at a resolution sufficient to loosely map stratigraphic contacts above the top of the "three finger" dolomite (at approximately 100 meters below ground surface). A key outcome was the evaluation of the relative difference in the rock properties above salt jugs, associated with the wells, compared to rocks above undisturbed salt. Comparisons of shear-wave velocity profiles over time (time lapse) provided insights into void dynamics and overburden stability.

Passive MASW data were continuously acquired over four nights (December 11 and 12, and December 16 and 17, 2019) focused above high priority wells on the Vigindustries site in Hutchinson, Kansas. A continuous sampling approach was used to record all available sources of passive source energy to ensure energy with optimal source orientation and surface-wave characteristics were captured for each line. Surface waves were recorded with frequencies as low as 3.5 hertz (Hz) representing an average depth of investigation of 65 meters (m) to more than 70 m, more than 50 m below the bedrock surface in many places.

Since shear modulus is the ratio of stress over strain and shear-wave velocity is a function of shear modulus and density, it is possible to estimate relative stress of overburden rocks (shear modulus) from shear-wave velocity values. Local increases in shear-wave velocity without changes in lithology can be equated to increased stress associated with changes in the loading of overburden roof rocks above dissolution jugs. Relative shear-wave velocity lows may be associated with collapse features whose vertical movement has been arrested by bulking, reduced stress to within roof rock strength, or changes in strength with vertical migration due to an encounter with different geologic features and properties related to natural variation in deposition or erosion.

Overall shear-wave velocity directly over or in proximity to most of the wells in this study represents natural geologic conditions and a normal stress regime. Therefore, the 2019 results suggest that the shale overburden is in a state of relative stability, as was also seen in 2018. Overburden materials above five wells from this December 2019 survey with notable changes in overburden characteristics are wells 2A, 4A, 7A, 15B, and 59.

- An abrupt 30% increase in velocity was observed at well 59 and an incremental 10% velocity increase was observed at well 15B. Continued monitoring for signs of incremental failure and void migration will provide insight into the source of these observed changes.
- A further 25% decrease in bulk velocity relative to 2018 was observed in a volume of rock along line 7, spanning wells 4A and 7A. Higher-mode interference and a 12% velocity decrease were observed in 2018 (relative to 2017), which suggested the

possibility of incremental failure and change in lithologic properties. The 2019 observations further support that possibility and suggest a reduction in bedrock competency. Absence of a low-velocity anomaly at depth suggests that no void has migrated within the sampled depth range and additional invasive investigation is not called for at this time.

- A slight reduction in bulk velocity at well 2A relative to the previous two years likely suggests a period of relative stability following a buildup in stress (elevated velocity in 2013), failure event and stress reduction (reduced velocity in 2014-2015), and subsequent rebound (return to near-native velocity in 2017-2018).

Introduction

Material properties (specifically strength and stress accumulations) measured as a function of depth above abandoned salt jugs in Hutchinson, Kansas, appear related to the mobility and upward migration potential of these jugs. Localized escalation in stress (as indicated by increased shear-wave velocity) above subterranean voids is one indicator of an increased potential for roof failure and void migration (Eberhart-Phillips et al., 1989; Dvorkin et al., 1996; Khaksar et al., 1999; Sayers, 2004). Previous studies, using both active and passive seismic wavefield characteristics, suggest perturbations in the shear-wave velocity field immediately above voids can be correlated to characteristics of the unsupported roof spans of salt jugs in the Hutchinson area (Sloan et al., 2010).

The strength of individual rock layers can be qualitatively described in terms of stiffness/rigidity and empirically estimated from relative comparisons of shear-wave velocity measurements. Shear-wave velocity is directly proportional to stress and inversely related to non-elastic strain. Since the shear-wave velocity of earth materials changes when stress and any associated elastic strain on those materials becomes "large," it is reasonable to suggest load-bearing roof rock above mines or dissolution voids may experience elevated shear-wave velocities due to loading between pillars or, in the case of voids, loading between supporting side walls. This localized increase in shear velocity is not related to increased strength but to increased load as defined by Young's Modulus. High-velocity shear-wave "halos" encompassing low-velocity anomalies are suggested to be key indicators of near-term roof failure. All these phenomena have been observed within the overburden above voids in the Hutchinson Salt Member in Hutchinson at depths greater than 30 m below the bedrock surface.

Previous research projects at the Carey Boulevard Research Area (CBRA) correlated measured shear-wave velocities with the condition of dissolution voids and the physical properties of the overburden at selected locations on Vigindustries legacy solution mining property in Hutchinson. In 2008, active seismic reflection was used to evaluate the effectiveness of shear-wave velocity to estimate local stress above voids of the size and depth prevalent at the Vigindustries site. It was determined that the integrity of the overlying strata could be reasonably estimated using shear-wave seismic imaging. The lack of necessary ultra-low-frequency surface waves in the recorded wavefield have negated attempts to use active-source multichannel analysis of surface waves (MASW) to estimate shear velocity in the lithified rocks near the top of bedrock (Miller et al., 2009).

Uncontrolled local industrial and transportation activities represent sound sources that have produced necessary low frequencies and, when recorded and processed using passive methods, have extended the imaging depth to more than 60 m (Miller, 2011). Key to this method is the ability to estimate shear-wave velocities to depths more than double those possible using

standard active sources at any particular site (Park et al., 2004). Results of passive MASW studies near this site suggest that this method is effective in identifying jugs with heightened risk for upward migration (Miller, 2011; Ivanov et al., 2013).

Following the active seismic imaging study in 2008, several two-dimensional (2-D) passive MASW surveys have been acquired at the CBRA (Table 1). Results of these investigations largely suggested a normal stress regime with natural geologic variation. In this study, passive MASW processing resulted in 12 2-D shear-wave velocity (Vs) profiles intersecting (or in proximity to) 40 wells. Individually, each profile represents a snapshot in time. When combined with previous observations at the same locations, time-lapse analysis can be used to monitor for temporal variation in shear velocity, providing insight into relative stability and void dynamics.

Table 1. Dates of and wells evaluated during 2-D passive MASW surveys at the CBRA.

Date	Wells
August 2012	2A, 1B, 2B, 3B, 5B, 6B, 7B, 12B
October 2012	2B, 4B, 6B, 17, 45, 52, 53, 59
March 2013	2A, 4B
November 2014	2A, 3B, 4B
March 2015	1B, 2B, 3B, 6B, 8A, 8B, 10B, 11B, 12B, 13B, 14B, 15B, 17, 18, 22A, 23, 23B, 29, 30, 39, 41, 42, 44, 45, 46, 86, 87, 88, 89, 90, 92
May 2015	2A, 4B
June 2015	4A, 6B, 7A, 7B, 52, 53, 59, 60
November 2017	2A, 4A, 7A, 8A, 1B, 2B, 3B, 4B, 6B, 7B, 8B, 10B, 11B, 12B, 13B, 14B, 15B, 17, 18, 22A, 23, 23B, 29, 30, 39, 41, 42, 44, 45, 46, 52, 53, 59, 60, 86, 87, 88, 89, 90, 92
October 2018	2A, 4B
December 2018	1B, 2B, 3B, 4A, 4B, 6B, 7A, 7B, 8A, 8B,10B, 11B, 12B, 13B, 14B, 15B, 17, 18, 22A, 23B, 23, 29, 30, 39, 41, 42, 44, 45, 46, 52, 53, 59, 60, 86, 87, 88, 89, 90
December 2019	1B, 2A, 2B, 3B, 4A, 4B, 5B, 6B, 7A, 7B, 8A, 8B, 10B, 11B, 12B, 13B, 14B, 15B, 17, 18, 22A, 23B, 23, 29, 30, 39, 42, 44, 45, 46, 52, 53, 59, 60, 88, 89, 90, 92

To further investigate and quantify the relationship between stress conditions and bulk-velocity changes over a void, a scaled physical model was designed using a moveable trapdoor (Terzaghi, 1936) in a large test box containing lightly compacted sand (Figure 1). The trapdoor descends vertically downward to simulate a collapsing void roof structure and changes in the in situ conditions were monitored with three different methodologies. In situ pressure changes in the sand column were measured continuously with buried pressure cells, multi-component surface-wave seismic surveys were conducted to image bulk velocity, and photogrammetry to visually monitor overburden displacement.

Although analysis of these datasets is still ongoing, preliminary results indicate a temporal increase in shear-wave velocity over the trapdoor (i.e. void) as the trapdoor moves vertically downward. The spatial distribution of this velocity increase is consistent with the gradual development of a tensional dome (Davies, 1951) observed directly above the trapdoor. According to the literature (Davies, 1951), the tensional dome forms above a void in response to a redistribution of stresses prior to roof failure and collapse. Preliminary data suggests the temporal increases in shear-wave velocity observed above the trapdoor (i.e. void) is consistent

with expected temporal changes in the stress conditions of the surveyed materials. This model is the first physical evidence supporting the analytical methods and interpretive concept that bulk-velocity changes observed over voids at the CBRA are related to variations in the stress conditions and material competency.

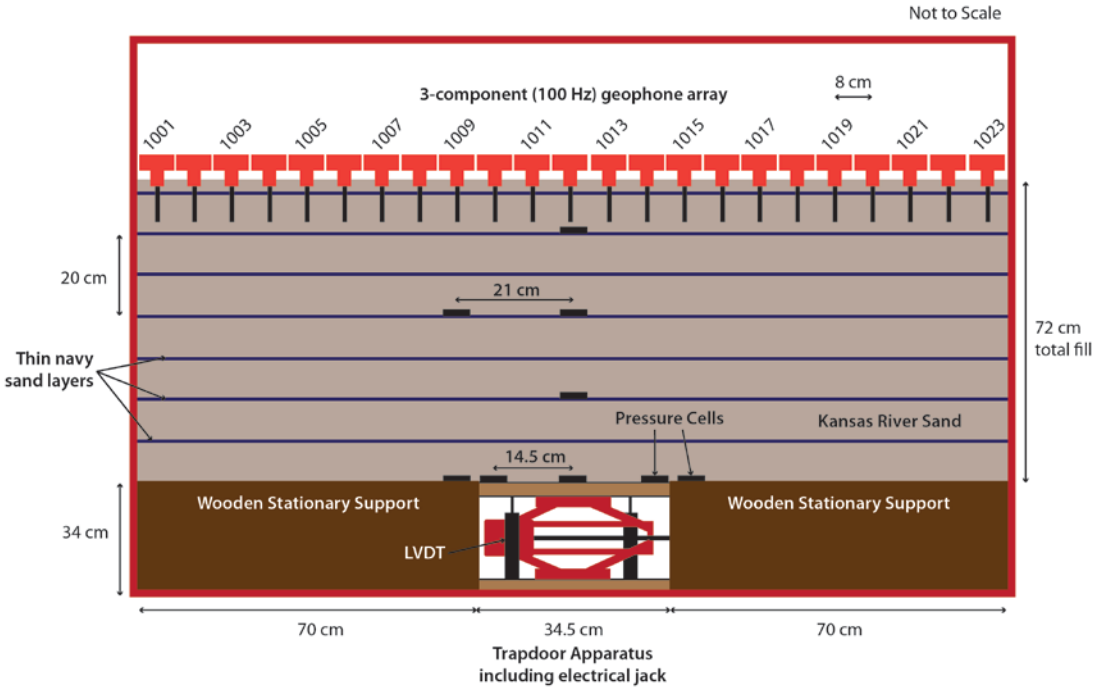

Figure 1. Illustration of physical model test setup including the moveable trapdoor, pressure cells, and geophone array across the surface of the sand test material.

Geologic and Geophysical Setting

The Permian-aged Hutchinson Salt Member occurs in central Kansas, northwestern Oklahoma, and the northeastern portion of the Texas panhandle and is prone to and has an extensive history of dissolution and formation of sinkholes (Figure 2). In Kansas, the Hutchinson Salt Member possesses an average net thickness of 75 m and reaches a maximum of more than 150 m in the southern part of the basin. Deposition occurring during fluctuating sea levels caused numerous halite beds, 0.2 to 3 m thick, to be formed interbedded with shale, minor anhydrite, and dolomite/ magnesite. Individual salt beds may be continuous for only a few miles despite the remarkable lateral continuity of the salt as a whole (Walters, 1978).

The distribution and stratigraphy of the salt is well documented (Dellwig, 1963; Holdoway, 1978; Kulstad, 1959; Merriam, 1963). The salt reaches a maximum thickness in central Oklahoma and thins to depositional edges on the north and west, erosional subcrop on the east, and facies changes on the south. The increasing thickness toward the center of the salt bed is due to a combination of increased salt and more and thicker interbedded anhydrites. The Stone Corral Formation (a well-documented seismic marker bed) overlies the salt throughout

Kansas (McGuire and Miller, 1989). Directly above the salt at this site is a thick sequence of Permian shale.

The upper 760 m of rock at this site is Permian shale (Merriam, 1963). The Chase Group (top at 300 m deep), lower Wellington Shale (top at 245 m deep), Hutchinson Salt (top at 120 m deep), upper Wellington Shale (top at 75 m deep), and Ninnescah Shale (top at 25 m deep) make up the packets of reflecting events easily identifiable and segregated within the Permian portion of the section (Figure 3). Bedrock is defined as the top of the Ninnescah Shale with the unconsolidated Pliocene-Pleistocene Equus beds making up the majority of the upper 30 m of sediment. The thickness of Quaternary alluvium that fills the stream valleys and paleosubsidence features goes from 0 to as much as 90 m, depending on the dimensions of the features.

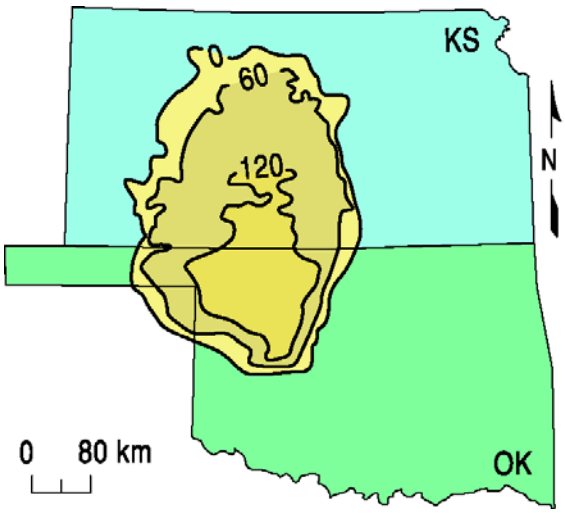

Figure 2. Approximate extent of salt formation, with contour intervals expressed in meters.

Recent dissolution of the salt and resulting subsidence of overlying sediments forming sinkholes has generally been associated with mining or saltwater disposal (Walters, 1978). Historically, these sinkholes can manifest themselves as a risk to surface infrastructure. The rate of surface subsidence can range from gradual to very rapid. Besides risks to surface structures, subsidence features potentially jeopardize the natural segregation of groundwater aquifers, greatly increasing their potential to negatively impact the environment (Whittemore, 1989, 1990). Natural sinkholes resulting from dissolution of the salt by localized leaching within natural flow systems that have been altered by structural features (such as faults and fractures) are not uncommon west of the main dissolution edge (Merriam and Mann, 1957).

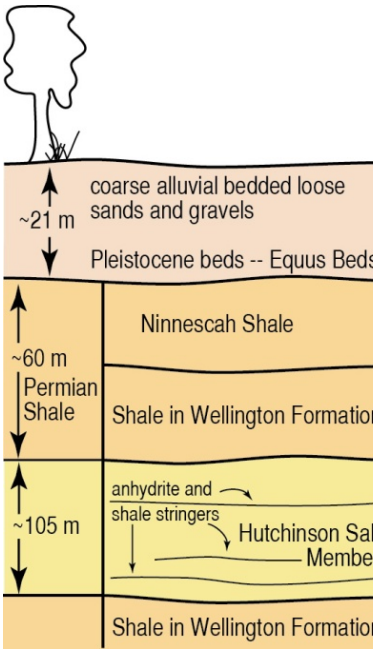

Figure 3. Generalized geology.

Caprock and its characteristics are a very important component of any discussion concerning dissolution, subsidence, and formation of sinkholes. The Permian shales (Wellington and Ninnescah) that overlay the Hutchinson Salt Member are about 60 m thick in this area and are characterized as generally unstable when exposed to freshwater, being susceptible to sloughing and collapse (Swineford, 1955). These Permian shales tend to be red or reddish-brown and are commonly referred to as "red beds." Permian red beds are extremely impermeable to water and have provided an excellent seal between the freshwaters of the Equus beds and the extremely water-soluble Hutchinson Salt Member. The modern-day expanse and mere presence of the Hutchinson Salt is due to the protection from freshwater provided by these red beds.

Isolating the basal contact of the Wellington Formation provides key insights into the general strength of roof rock expected, if dissolution-mined salt jugs (salt jugs are the jug-shaped

cavities or voids in the salt that form after salt has been dissolution mined in proximity to the wells) reach the top of the salt zone. Directly above the salt/shale contact is approximately 6 m thick dark-colored shale with joint and bedding cracks filled with red halite (Walters, 1978). Once unsaturated brine comes in contact with this shale layer, these red halite-filled joints and bedding planes are rapidly leached, leaving an extremely structurally weak layer.

Field Layout and Data Acquisition

To ensure the highest quality data, receivers were deployed during daylight hours and train data recorded at night when cultural and industrial noise was minimal to provide optimum signal-to-noise ratio. Analysis of previous seismic energy sources captured during passive recording at this site clearly indicated trains at distances of 3 kilometers (km) or more provided the best broad spectrum, low-frequency seismic energy (Miller, 2011). Since seismic energy with characteristics best suited for this study may arrive when trains are at distances greater than can be detected by spotters, seismic energy was recorded continuously throughout the night to ensure the capture of times possessing optimum data.

Data were acquired over four nights, December 11 and 12, and December 16 and 17, 2019. A total of twelve seismic lines were deployed collectively over the four nights. Line layout was designed to cross directly over all wells of interest. A 2-D grid of receivers (Figure 4) designed to monitor incident orientation of passive seismic energy (Figure 5) was active throughout the four nights of the survey. Seismic receivers were single ION 4.5 Hz geophones spaced at 3 m intervals. The seismic lines collectively totaled approximately 4485 m in length. The 2-D monitoring/ alignment grid consisted of 131 receivers spaced at 5 m intervals and was configured to form four concentric expanding squares with 10, 30, 50, and 70 m sides. Data were recorded with a 400+ channel 24-bit Geometrics Geode distributed seismic system. Seismic records were 30 seconds (s) long with a 2 millisecond (ms) sampling interval. In total, 3676 seismic records were recorded, which resulted in 110 gigabytes (Gb) of data.

Processing and Analysis

Data were processed using algorithms developed at the Kansas Geological Survey (KGS). The passive method used for this study is well published and has consistently proven effective producing good-quality results (Park et al., 2004; Ivanov et al., 2013). The continuous-data-acquisition method records energy from nearby sources at various orientations with respect to the seismic line. Data from the 2-D grid are evaluated for optimized source alignment with respect to each 1-D seismic line allowing data rotation or analysis of only data from near in-line sources.

For each line, the surface-wave amplitudes recorded by the 2-D grid were plotted as phase velocity versus frequency across a range of azimuths, from 0 to 360 degrees relative to the seismic line, to identify which record had the best broad-band, low-frequency source energy with an azimuth as near zero as possible (Figure 6). Seismograms for each line with optimum source characteristics were selected and segmented into the shortest groups of receivers ("spread length") that provided dispersion patterns on phase velocity versus frequency plots with the greatest per-centage of high amplitude fundamental mode Rayleigh-wave energy with minimal higher-order surface-wave interference (Figure 7).

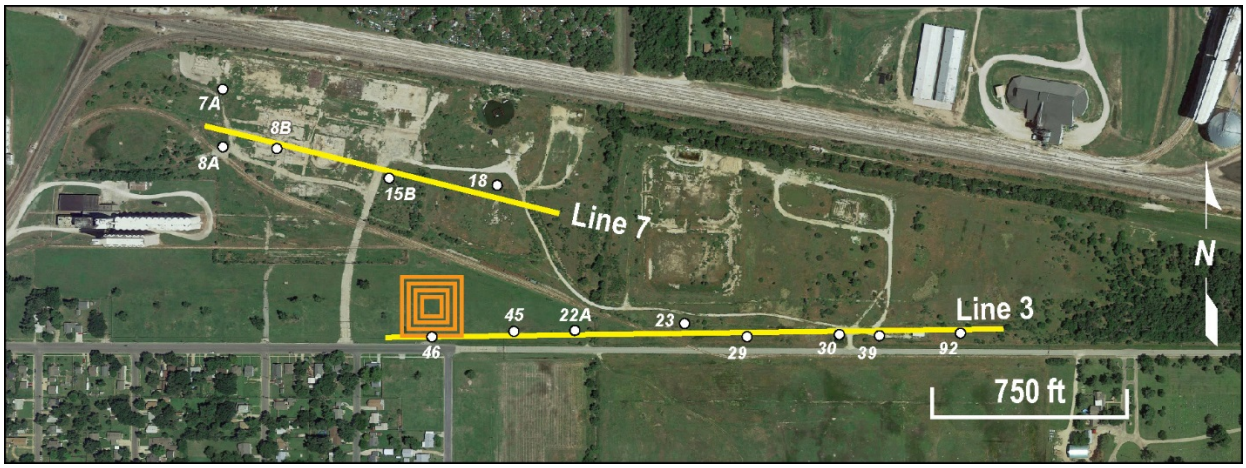

Figure 4. Aerial photo with GPS locations of 2-D grid of receivers (orange squares) with respect to acquisition of lines 7 and 3.

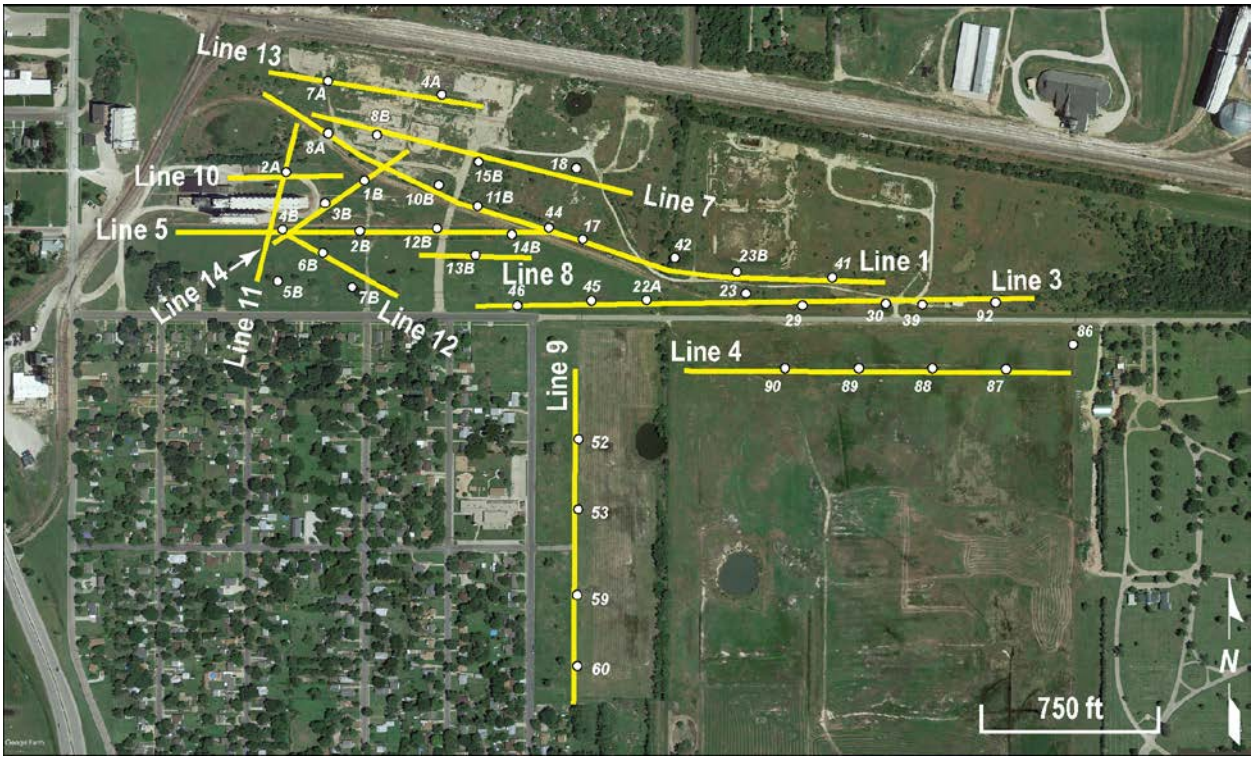

Figure 5. Aerial photo with GPS locations of seismic lines and wells in the study area.

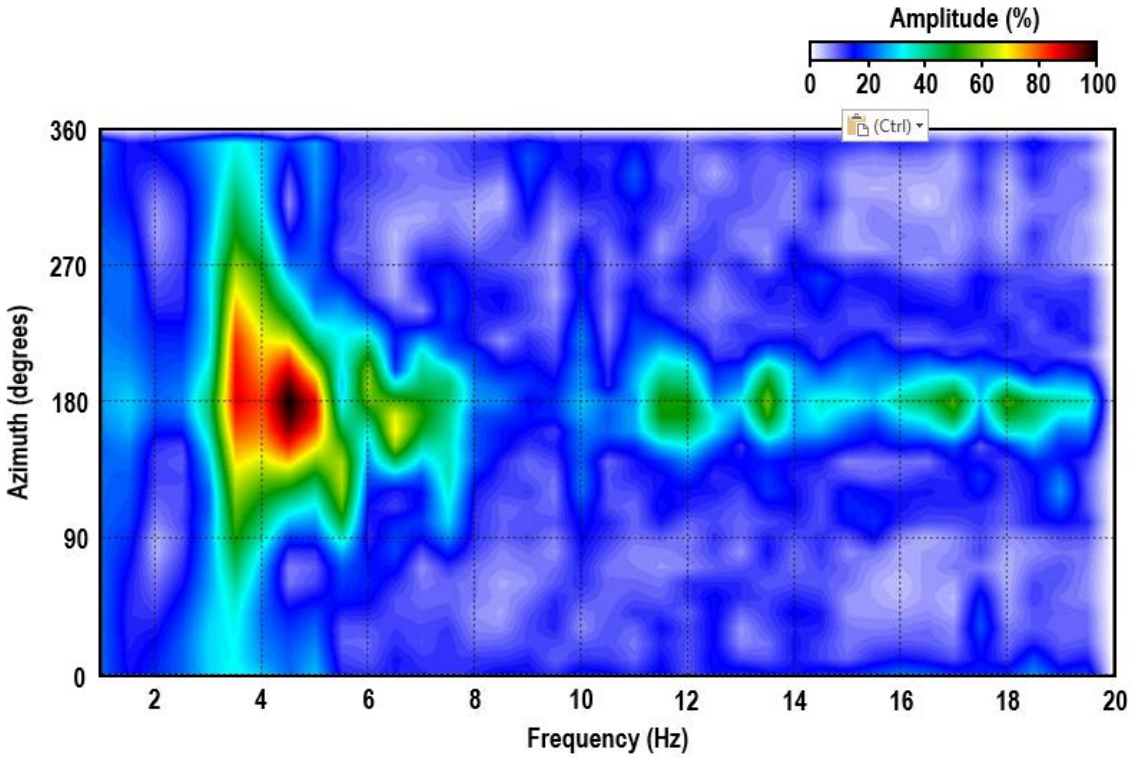

Figure 6. Azimuth plot indicating the direction of the dominant passive source energy (in degrees counter-clockwise from east). Here, the dominant passive source energy is centered on approximately 180°.

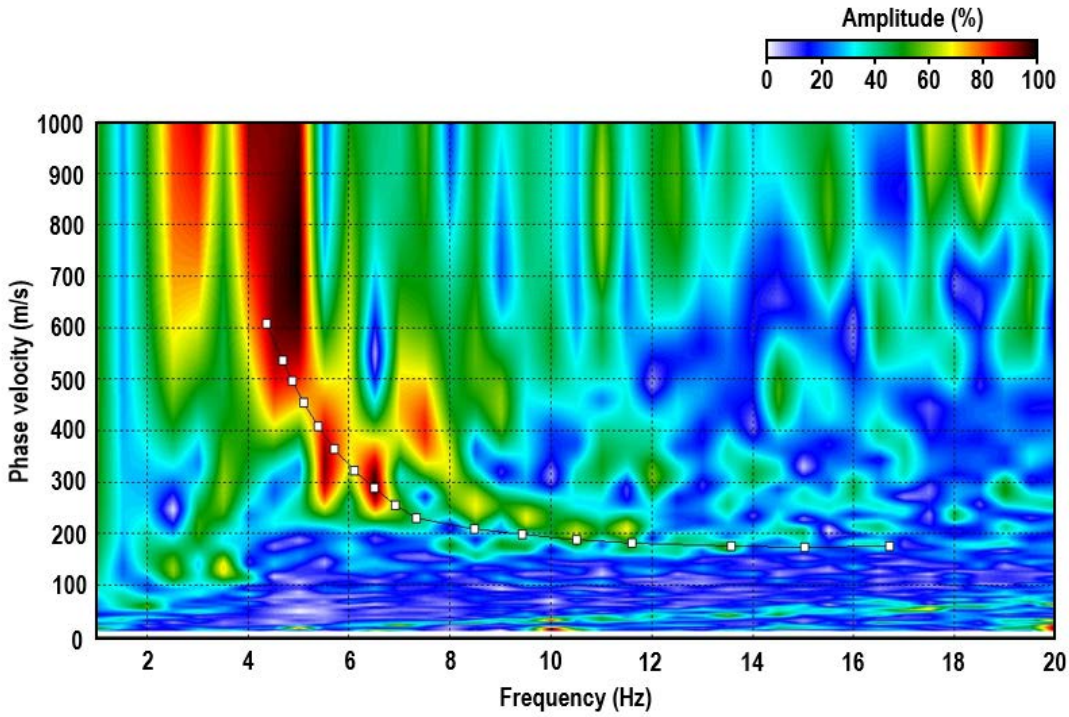

Figure 7. Dispersion pattern with high signal-to-noise ratio of the fundamental mode Rayleigh wave.

Fundamental mode dispersion curves were picked and inverted to obtain a 2-D section of shear-wave velocity as a function of depth. The apparent velocity (v_{app}) is:

$$v_{app} = \frac{v_{act}}{(\cos\theta)} \tag{1}$$

where v_{act} is the actual seismic velocity and θ is the azimuth of the source with respect to the seismic line determined from the azimuth versus frequency plot. Thus, the percent increase in velocity (Δv) is:

$$\Delta v = \frac{1}{\cos\theta} - 1 \tag{2}$$

Equation 2 was used to calculate the increase in velocity due to the source azimuth for each line (Table 2).

Table 2. Directions of the passive seismic sources and the seismic lines; spread length used for processing, the angle of the source with respect to the line (θ, in degrees counterclockwise from east), and the percent increase in apparent velocity (Δv) attributable to oblique source orientations.

	processing spread length(s)	source orientation	line orientation	θ	Δv
line 1	102 m 102 m	138° 150°	135° 180°	3° 30°	< 0.14% < 15.45%
line 3	105 m, 120 m	180°	180°	0°	0%
line 4	96 m	180°	180°	0°	0%
line 5	114 m	180°	178°	2°	< 0.06%
line 7	84 m	158°	165°	7°	< 0.75%
line 8	75 m	180°	176°	4°	< 0.24%
line 9	84 m	88°	86°	2°	< 0.06%
line 12	72 m,102 m	203°	207°	4°	< 0.24%
line 13	96 m	149°	172°	23°	< 8.63%
line 14	99 m	32°	35°	3°	< 0.14%

Results and Observations

Line 1

The NW-E oriented line 1 has a slight curvature and extends across wells 8A, 10B, 11B, 44, 17, 42, 23B, and 41 (Figure 8). The upper 10-15 m have an estimated average velocity of 175 m/s, which is consistent with previous years as well as the shear-wave velocity of unconsolidated sediments expected at this site. Depth to bedrock is approximately 20-25 m as indicated by the velocity gradient depth. The average depth of investigation along line 1 is ~70 m, which is 15 m greater than 2018, which is generally consistent with the 2017 survey result.

Due to the nonlinear alignment of line 1, data were processed using two different source azimuths (Table 2) to minimize apparent velocity calculations and maximize inline signal quality necessary for imaging high-amplitude dispersive trends. After targeted filtering to reduce an interfering higher mode, coherent fundamental-mode trends were observed from stations 1018-1150 (Figure 9a); amplitudes were relatively decreased between stations 1113-1125 (Figure 9b), but this station range coincides with the curved deployment of the array. Higher-mode interference affected the coherency of the fundamental-mode trend from 6-9 Hz for stations 1150-1170, but low-frequency information could still be retrieved down to 3.5 Hz (which corresponds to approximately 80 m depth).

In 2019, seven fewer receivers were deployed on the southeastern end of line 1. This in conjunction with the longer spread length used to produce low-frequency dispersive trends (102 m in 2019 vs. 87 m in 2018) accounts for well 41 not being reached with 2019 surface-wave inversion results. East of station 1244, frequency information would not be picked below 4.5 Hz (Figure 9c), which limited the depth of investigation to an average 50 m in this section of the survey line. Overall, the bulk-velocity trend is consistent with the previous 2018 survey and does not indicate any areas of concern with respect to shale bedrock competency above the surveyed wells.

Line 3

Line 3 is oriented W-E and intersects wells 46, 45, 22A, 23, 29, 30, 39, and 92 located approximately at stations 3025, 3057, 3080.5, 3124, 3148, 3183.5, 3199, and 3230.5, respectively (Figure 10). As expected in this region and unconsolidated sediment, the upper 15 m has an average shear-wave velocity of 175 m/s. The velocity gradient observed at 20 m depth indicates the top of shale bedrock. With the exception of stations 3065-3075, the maximum depth of investigation achieved was at least 70 m throughout a majority of line 3; stations east of well 39 (i.e., station 3199) had 70-85 m of inverted depth information. Overall, the bulk-velocity trend produced in 2019 (Figure 10d) is consistent with previous investigations along line 9 and represents a normal stress regime.

High-amplitude higher-mode energy did interfere with the fundamental-mode trend in portions of line 3 in the 4-7.5 Hz frequency range. This lack of low-frequency signal was overcome with advanced processing schemes that marginally improved the signal-to-noise ratio of the fundamental mode between 5-8 Hz for station range 3053-3075. For stations 3076-3207, a longer spread length (i.e. 120 m vs. the 105 m spread used for westernmost and eastern most stations) was required to produce a more easily-interpretable fundamental-mode trend with reduced interference from higher-mode energy. Although dispersive trends were attenuated between stations 3125 and 3175, but the dispersive information available was adequate enough to complete data processing throughout this challenging central section of line 3.

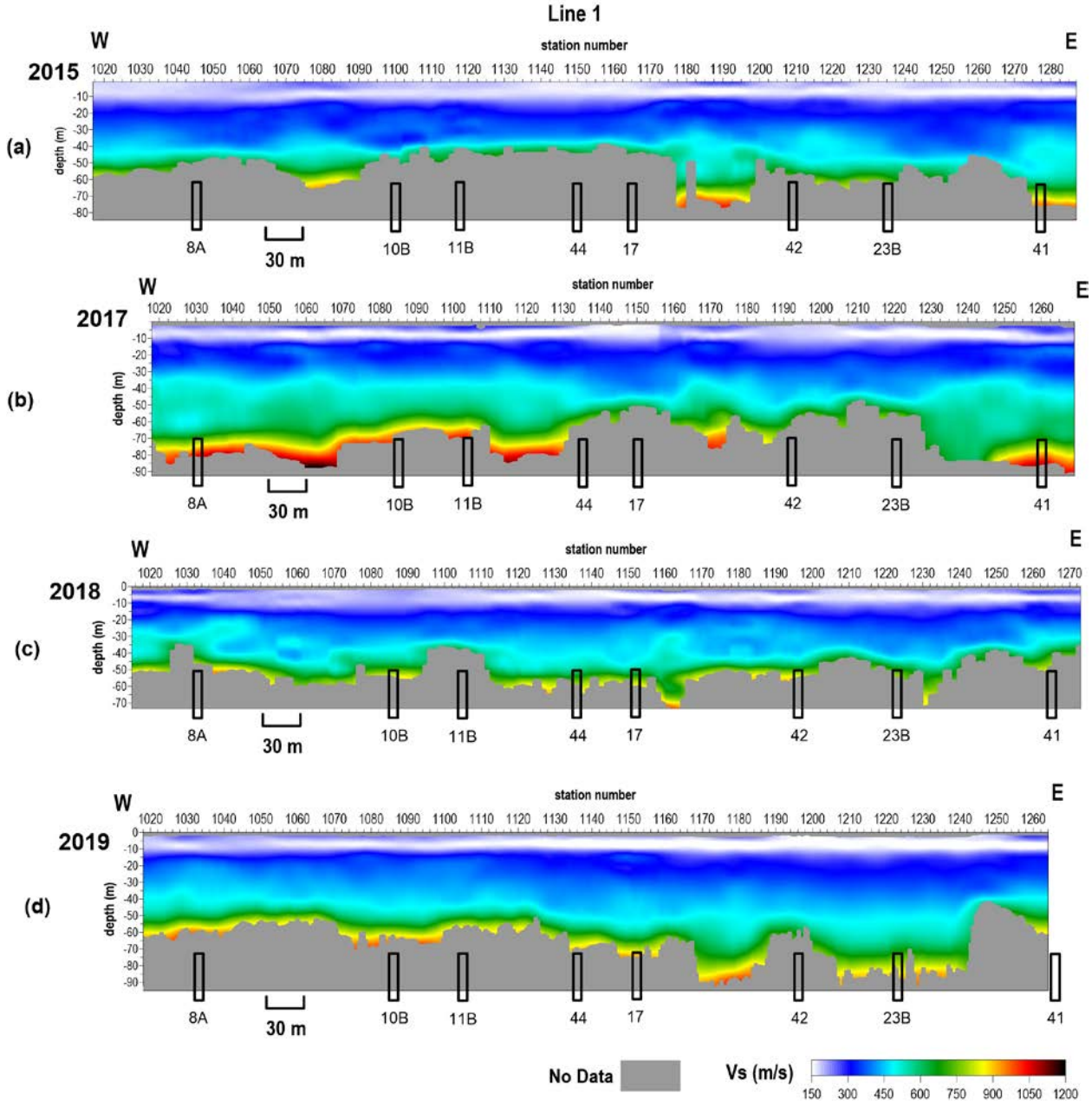

Figure 8. Shear-wave velocity profiles from line 1 from (a) March 2015, (b) November 2017, (c) December 2018, and (d) the current December 2019 investigation with approximate well locations.

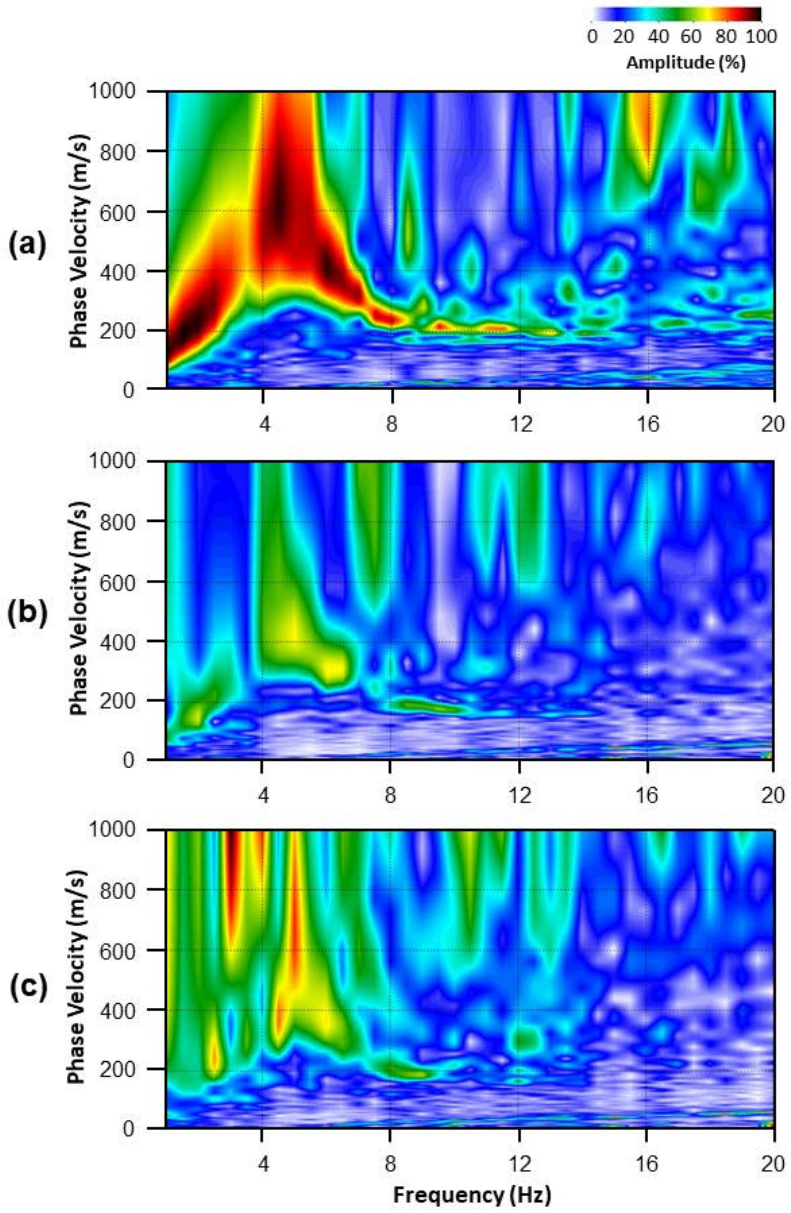

Figure 9. Example dispersion-curve images from stations (a) 1032, (b) 1118, and (c) 1250 that display varying levels of fundamental-mode coherency along line 1.

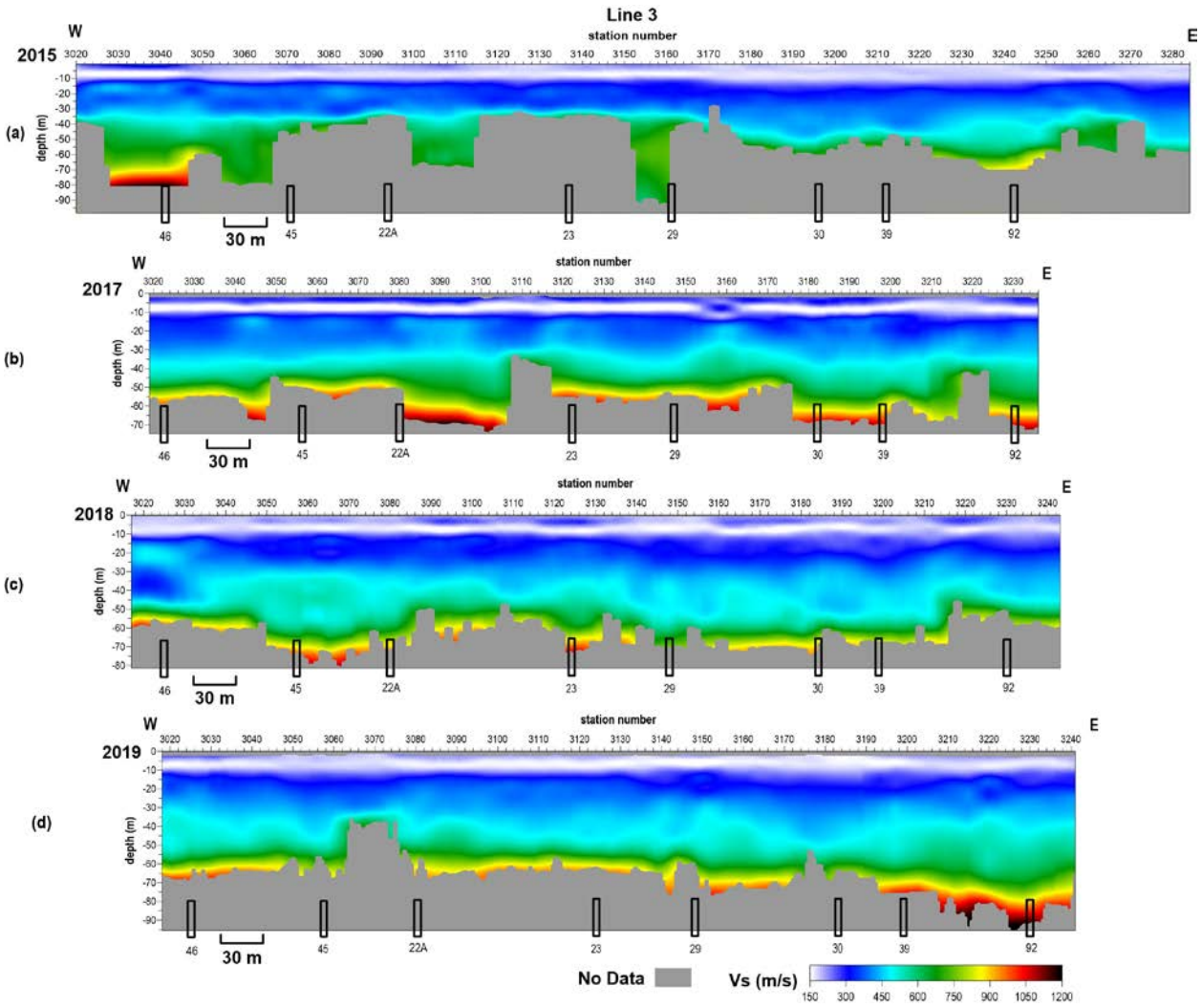

Figure 10. Shear-wave velocity profiles from line 3 from (a) March 2015, (b) November 2017, (c) December 2018, and (d) the current December 2019 investigation with approximate well locations.

Line 4

Line 4 is oriented W-E and covers wells 90, 89, 88, and 87 at stations 4044, 4076, 4707.5, and 4139.5, respectively (Figure 11). The upper 15 m has an average velocity of 175 m/s, which is consistent with unconsolidated sediment documented in this area. Overall, the 2019 bulk-velocity structure is consistent with the 2018 result between the westernmost station 4016 and eastern station 4707 (i.e. well 88). Similarly to the 2018 survey (Figure 11c), spread lengths used for 2019 processing did not extend to stations that overlap with the location of well 87. Nonetheless, inverted velocities from stations adjacent to well 87 are consistent with the bulk-velocity trend observed throughout line 4. This normal stress regime differs from the 2018 survey where stations nearest to well 87 exhibited elevated velocities (~15%) between 35-75 m depth relative to the rest of the 2018-line 4 result.

Fundamental-mode trends in 2018 were reported to be significantly less coherent between stations 4120-4130 (i.e. near well 87) which could account for this elevated velocity anomaly. Given the decreased signal-to-noise ratio, higher-mode energy could have been mis-interpreted as the fundamental-mode trend; this mode misidentification would account for the elevated velocity anomaly in 2018. However, fundamental-mode trends in 2019 were relatively consistent throughout line 4 with high-quality recorded source signal. Between stations 4037-4057, low-frequency information below 4.5-5 Hz was limited and subsequently resulted in shallower depths of investigation. At this time, the bulk-velocity structure shown in Figure 11d from 2019 represents a normal stress regime, but additional geophones may be required in future deployments to better investigate the area surrounding line 87.

Line 5

Line 5 is oriented W-E and intersects wells 4B, 2B, 12B, and 14B at stations 5027.5, 5061, 5094, and 5126.5, respectively (Figure 12). Shear-wave velocities observed in the upper 15 m are approximately 175 m/s, as expected for unconsolidated sediments, followed by a velocity gradient at 20 m depth, which indicates the top of shale bedrock. A longer optimal spread length (i.e. 114 m) was required for 2019 data processing compared to previous years (93-105 m) in order to achieve the maximum depth of investigation shown in Figure 12d. Despite the use of a longer spread in the current study, the depth of investigation was shallower by approximately 10 m with respect to the 2018 result for all stations east of station 5045. For stations west of 5045, which includes the location of well 4B, the maximum depth achieved was consistent with the previous study. Dispersion-curve trends also exhibited the highest signal-to-noise ratio in this station range (Figure 13a) compared to the rest of line 5 (Figure 13b). Although higher-mode energy interrupted the fundamental-mode trend between stations 5050 and 5070, the bulk-velocity trend of line 5 is generally consistent with previous surveys.

Line 7

Line 7 is oriented NW-SE and extends across wells 8B, 15B, and 18 located approximately at stations 7027, 7072, and 7113, respectively (Figure 14). The upper 15 m has an average shear-wave velocity of approximately 175 m/s, which is consistent with unconsolidated materials. The top of bedrock is observed at around 15 m depth as indicated by the large velocity gradient. An 84 m spread was used for processing in 2019, which was shorter than previous years that were over 100 m long. A transition zone was observed in the fundamental-mode trends near station 7035 from a higher to lower phase-velocity trend, but the bulk-velocity trend remained relatively consistent in this area due to the change in frequency content.

Although dispersion-curve interpretation was more challenging in previous years, fundamental-mode trends were confidently picked in 2019 with minimal higher-mode interference from 3.5-18 Hz. This resulted in an average 75 m depth of investigation. Through additional interpretation of line 7, it was determined that previous surface-wave trends were more challenging due to aliasing from source signal from an azimuth different from previously thought. The true velocity structure for 2018 was readjusted to more accurately account for apparent velocity estimation and the new 2018 Vs profile is shown in Figure 14c. Given this re-estimation, the 2019 bulk-velocity trend (Figure 14d) is generally consistent with observations from previous years. However, greater inverted depth was achieved between stations 7075-7100, or east side of well 15B, as well as a 10% increase in shear-wave velocity between 40-80 m depth. These observations may suggest a changing velocity structure has been occurring near well 15B since 2015.

Line 8

Line 8 is oriented W-E and intersects well 13B at station 8025 (Figure 15). The velocity of the upper layer is approximately 175 m/s, which, like the other lines on this survey, is consistent with the shear-wave velocity of unconsolidated sediment local to this area. The top of shale bedrock is indicated by the large velocity gradient observed at approximately 15 m depth. Coherent and high-amplitude dispersive trends were observed across line 8. Inversion results from 2019 are generally consistent with the bulk-velocity trends observed in previous years (Figure 15) indicating no change in the apparent strength or consistency of the shale overburden. The maximum depth of investigation was limited to 55 m from station 8029-8035 due to the lower velocity trend interpreted for the fundamental mode.

Line 9

Line 9, which is parallel to Williams Street, is oriented N-S and intersects wells 52, 53, 59, and 60 (Figure 16). The upper 15 m has an average shear-wave velocity of approximately 175 m/s, again consistent with the expected conditions at this site. The top of shale bedrock is indicated by the large velocity gradient at approximately 20 m depth. Interestingly, a shorter optimal spread (84 m vs. 114 in 2018) provided adequate wavelengths to achieve an 85 m average depth of investigation, which was 20 m greater than previous investigations. However, it is important to keep in mind that wavelength is also a factor of other seismic properties such as velocity. As a result, the bulk-velocity structure in 2019 (Figure 16d) exhibited an estimated 20% increase between 30-50 m depth since 2018 (Figure 16c), and only an 8% increase since 2017 (Figure 16b). An anomalous elevated velocity feature is observed between stations 9070-9105 at depths greater than 50 m (Figure 16d); well 59 is also located within this station range.

The fundamental-mode trend (Figure 17a) was discontinuous with decreased energy amplitudes in the same station range as this anomalous velocity zone on line 9; decreased energy amplitudes were observed in other sections of line 9, but the fundamental-mode trend was more continuous (Figure 17b) compared to this anomalous zone. Although ambient-noise methods have variable signal quality (e.g. energy amplitudes, frequency content), the absence of coherent signal can also be attributed to the measured geologic environment if the stress conditions are changing. Low signal-to-noise ratio of the fundamental mode was observed in the 2018 results, but the elevated velocity anomaly in the current study is approximately 30% higher than reported for stations surrounding well 59. Given that this is the first indication of elevated velocity on

line 9 in recent years, it is possible that this is related to changes in the shale bedrock competency, but additional monitoring is required to better evaluate the stress conditions.

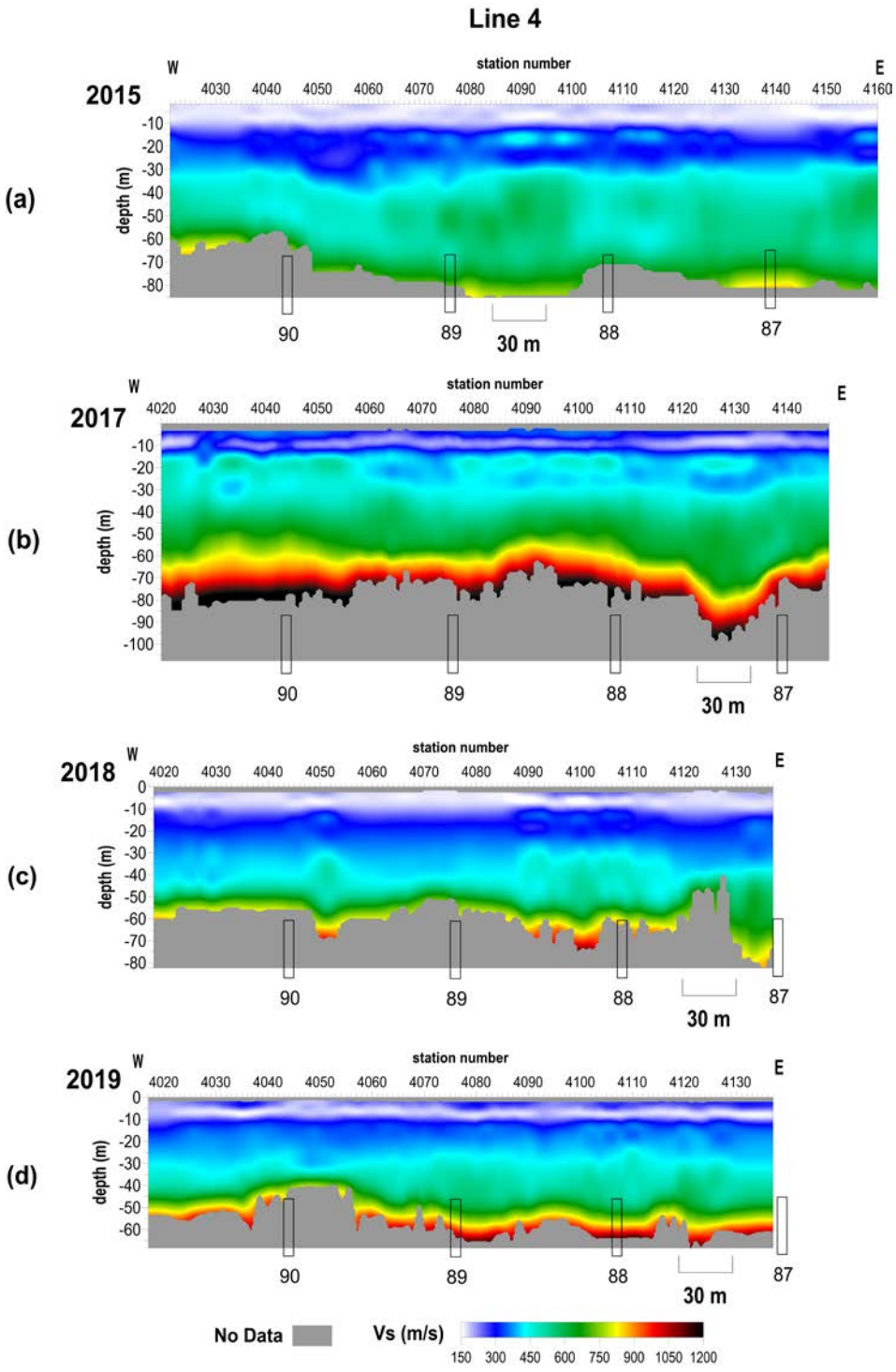

Figure 11. Shear-wave velocity profiles from line 4 from (a) March 2015, (b) November 2017, (c) December 2018 and (d) the current December 2019 investigation with approximate well locations.

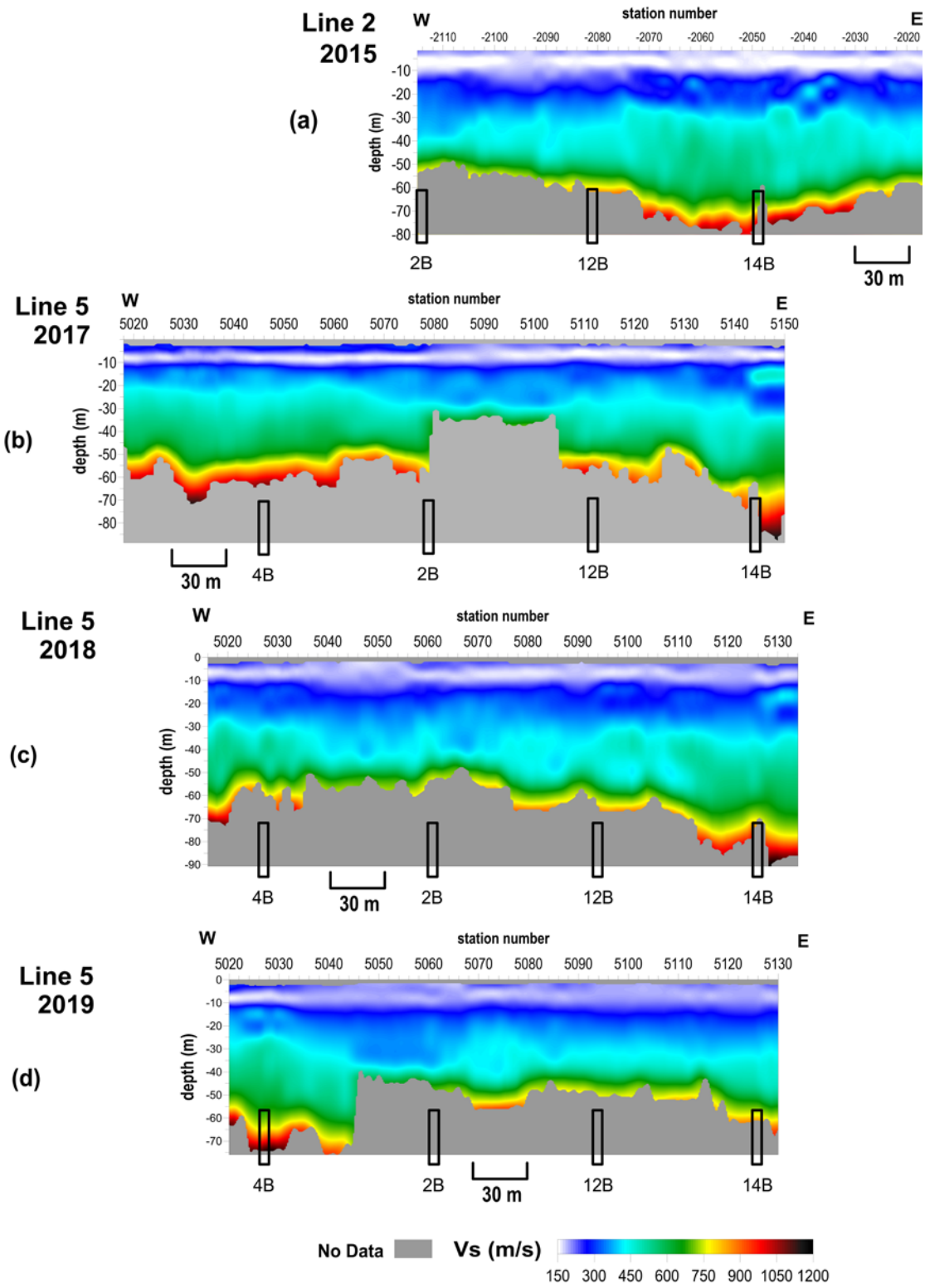

Figure 12. Shear-wave velocity profiles from line 5 from (a) March 2015 [named line 2 on the 2015 survey], (b) November 2017, (c) December 2018, and (d) the current December 2019 investigation with approximate well locations.

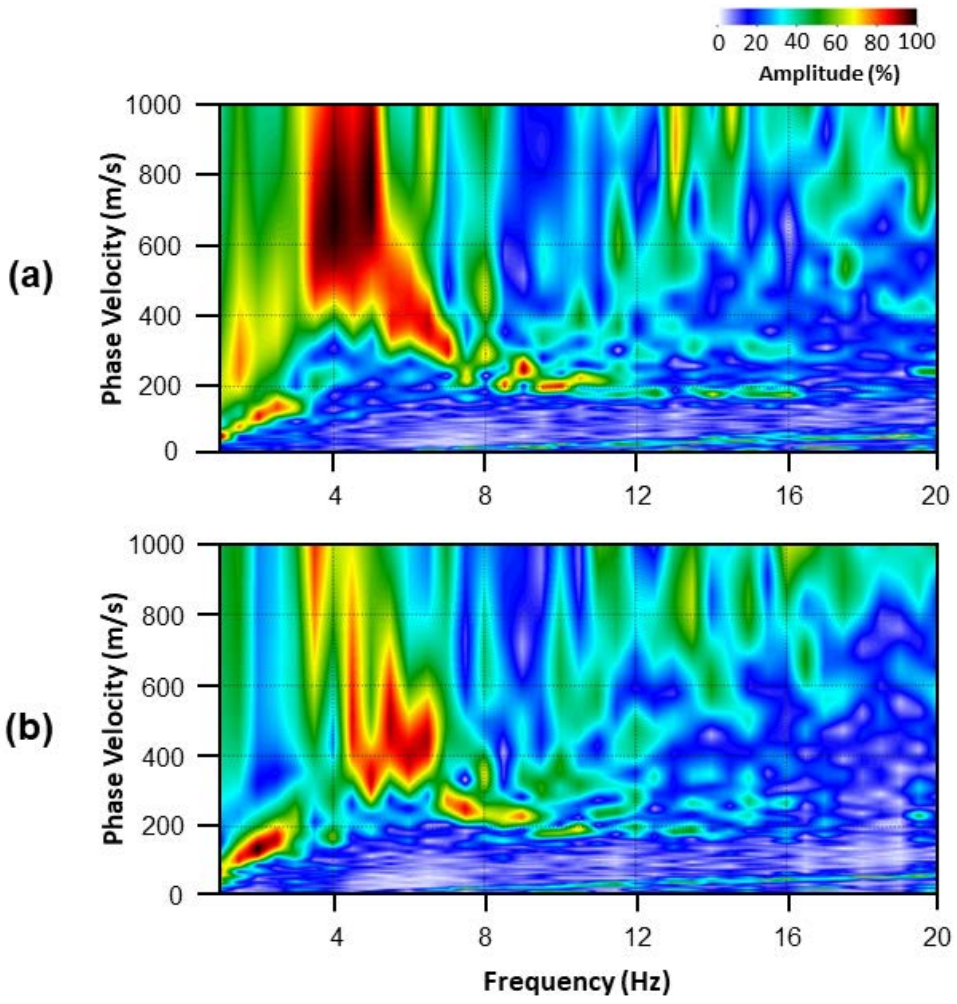

Figure 13. Example dispersion-curve images from (a) station 5031 near well 4B and (b) station 5062 that exhibit varying levels of fundamental-mode coherency along line 5.

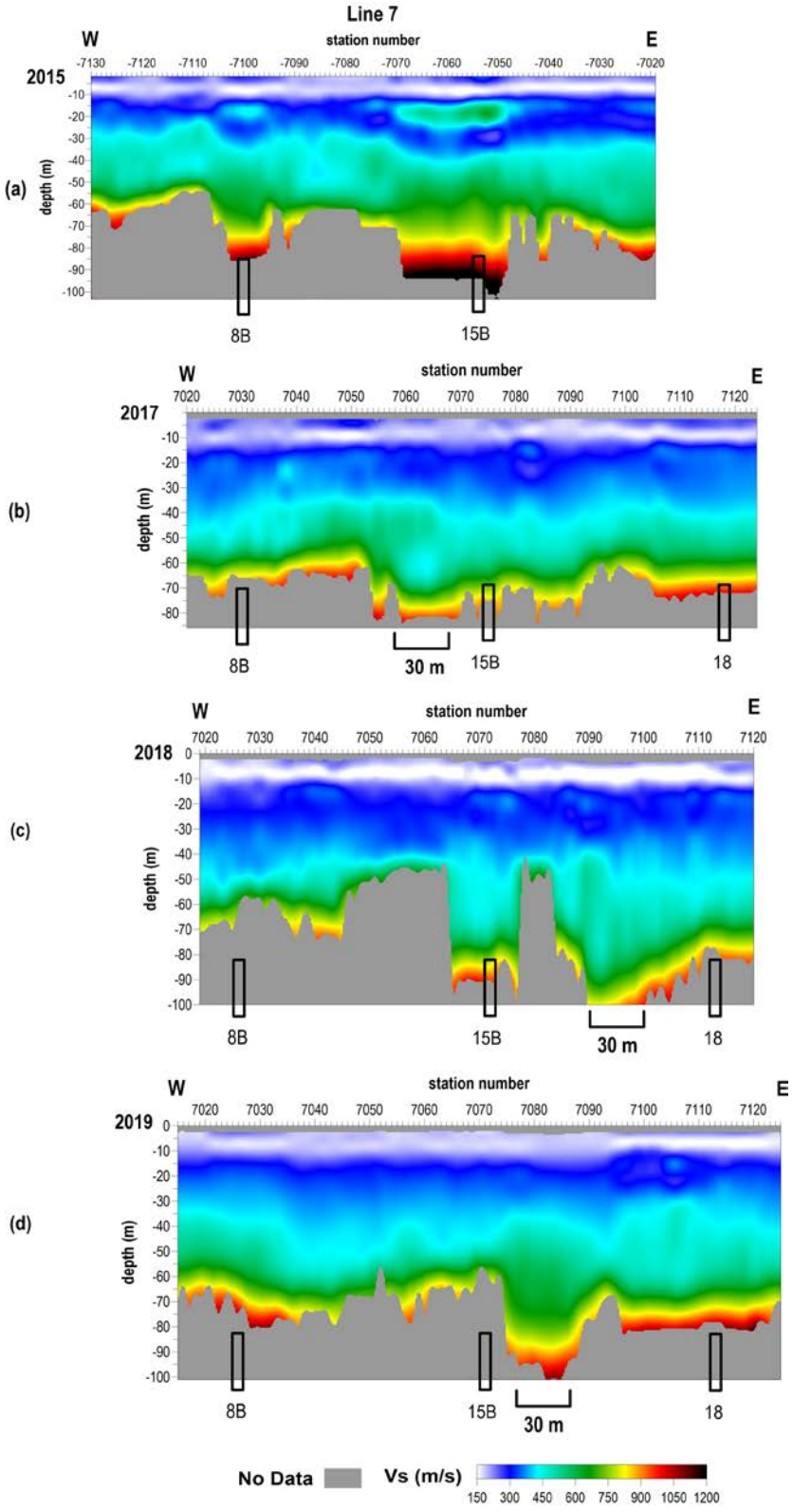

Figure 14. Shear-wave velocity profiles from line 7 from (a) March 2015, (b) November 2017, (c) December 2018, and (d) the current December 2019 investigation with approximate well locations.

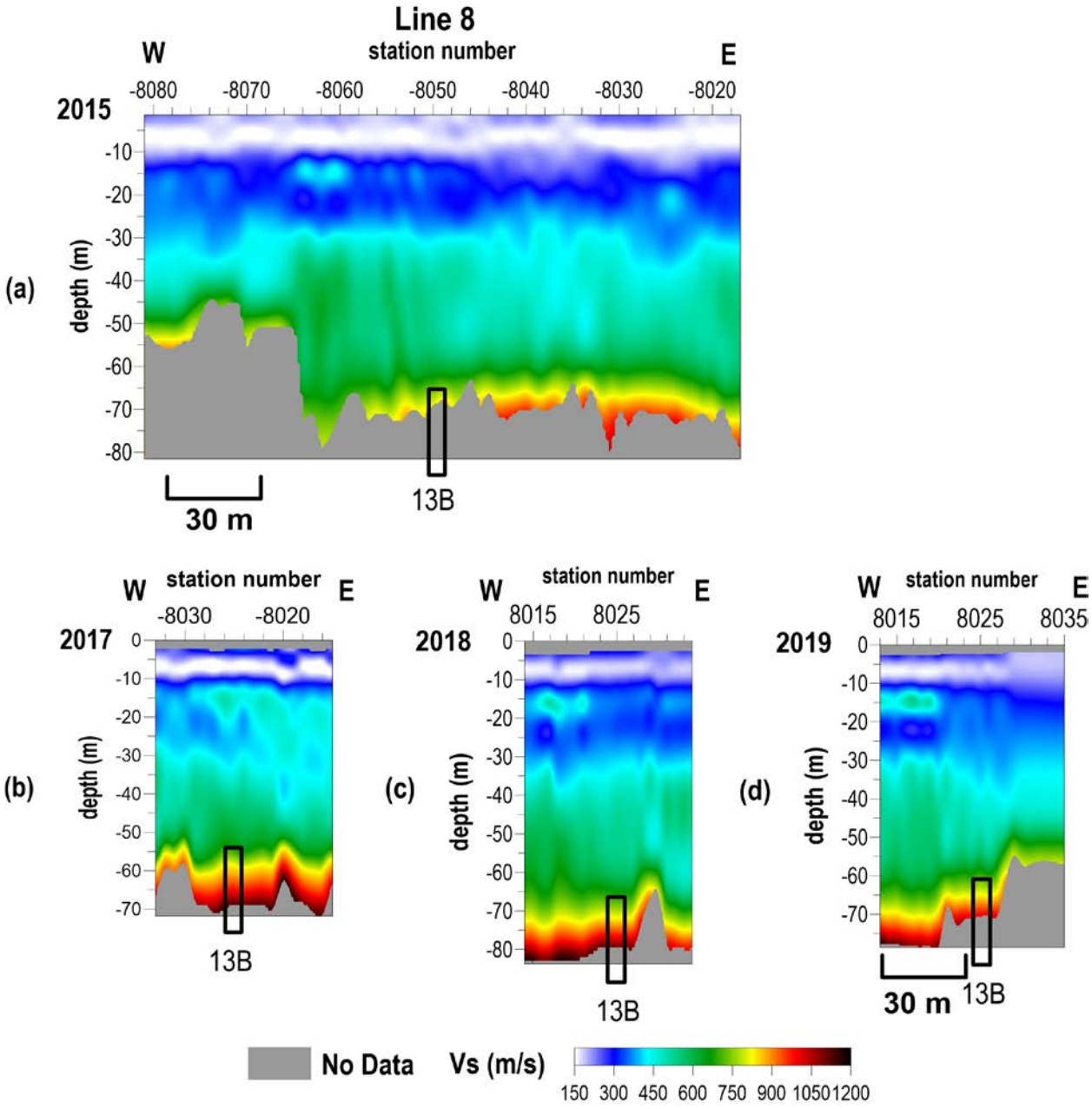

Figure 15. Shear-wave velocity profiles from line 8 from (a) March 2015, (b) November 2017, and (c) the current December 2018 investigation with approximate well locations.

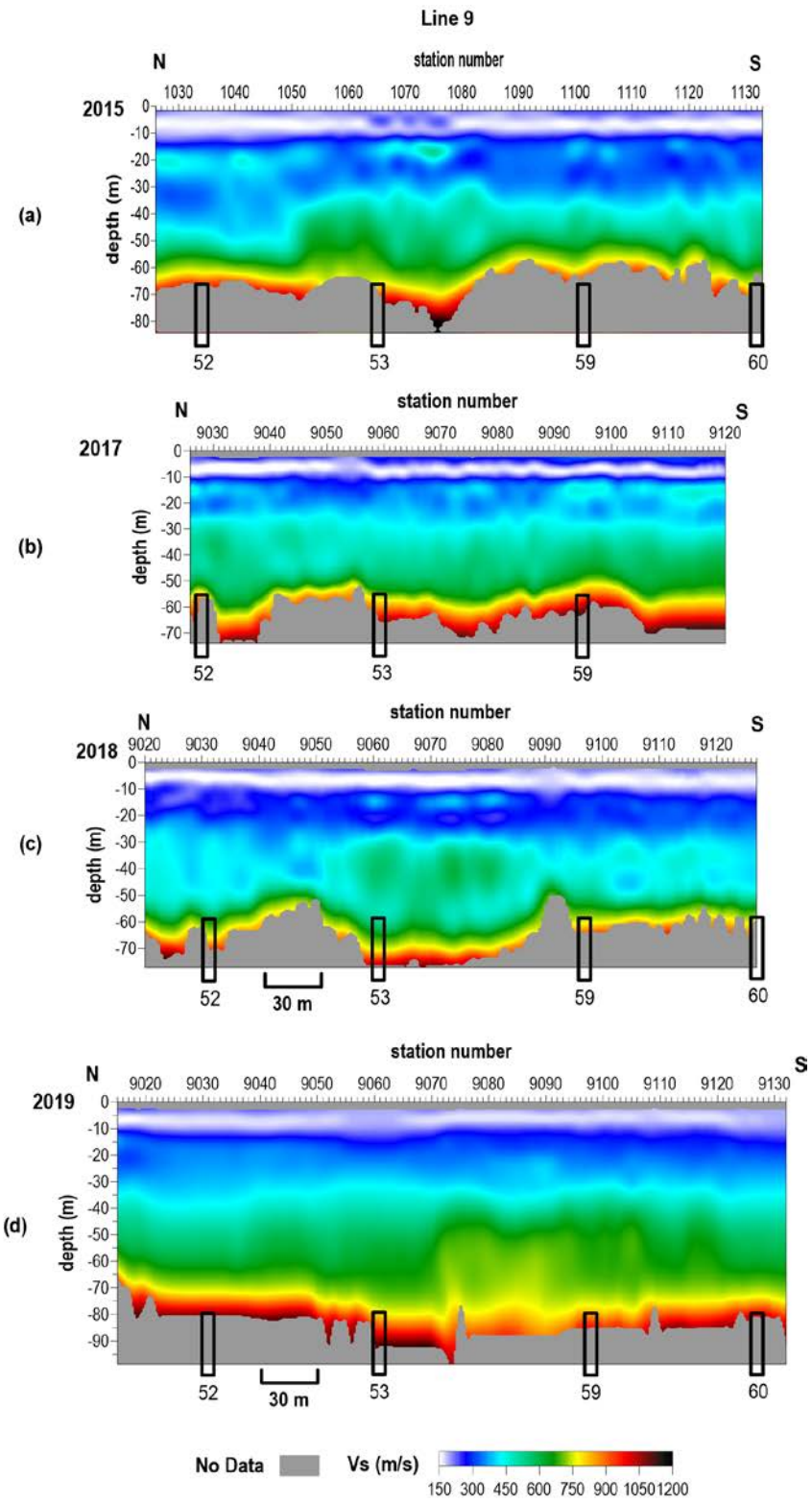

Figure 16. Shear-wave velocity profiles from line 9 from (a) March 2015, (b) November 2017, (c) December 2018, and (d) the current December 2019 investigation with approximate well locations.

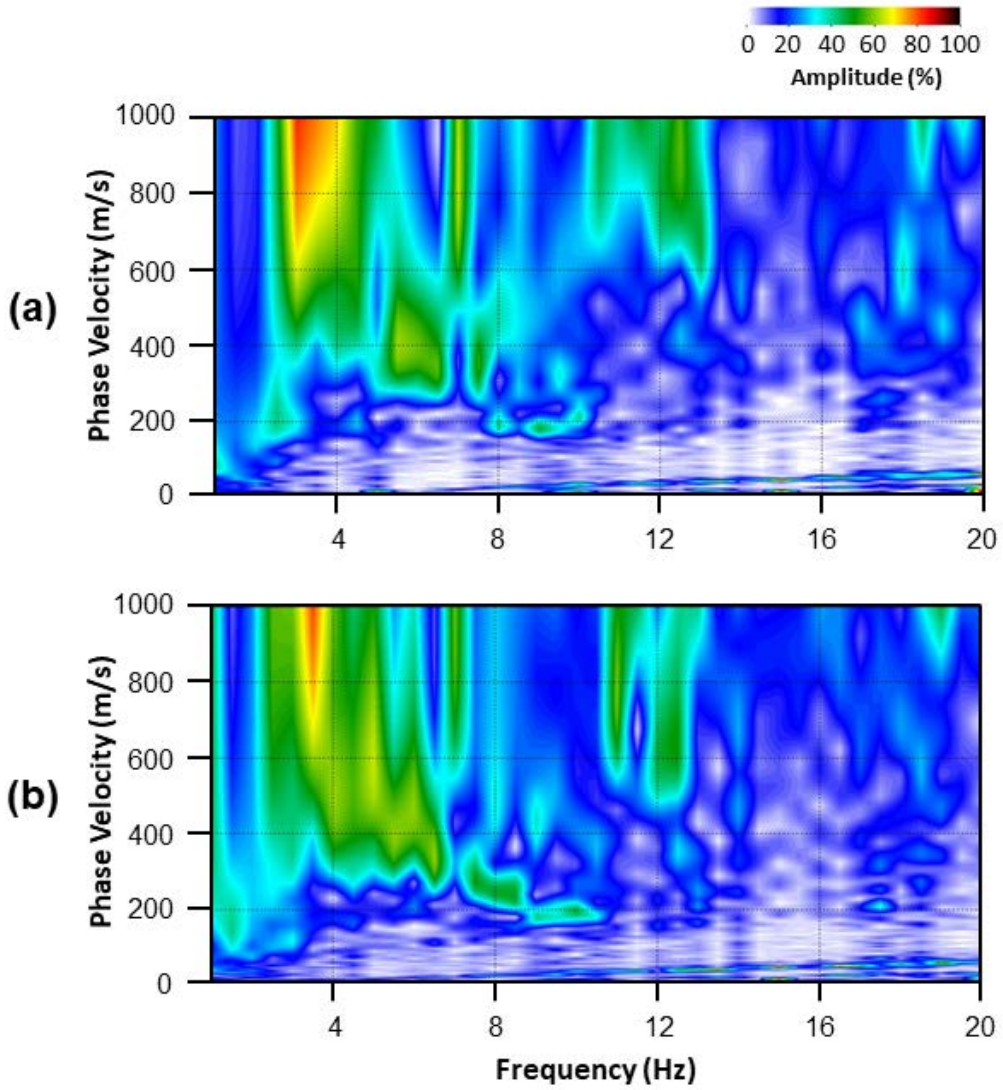

Figure 17. Example dispersion-curve images from line 9 where (a) station 9084 exhibited increased signal attenuation compared to (b) station 9060 which exhibited a more continuous fundamental-mode trend.

Line 10

Line 10 is a W-E oriented line that crosses well 2A at station 1022 (Figure 18). The average velocity of the upper 15 m is approximately 175 m/s, consistent with the unconsolidated sediment expected in this area. The velocity gradient at 15 m indicates the interface between the unconsolidated sediment and shale bedrock. Signal quality of the fundamental-mode diminished from eastern to western stations such that dispersive trends observed on the eastern end were higher amplitude and more continuous than western dispersive trends (Figure 19). This change in signal quality occurred at stations consistent with the location of well 2A where a decrease in both maximum depth of investigation and bulk velocity also occurs (Figure 18f). Shear-wave velocity profiles from 2017 (Figure 18d) and 2018 (Figure 18e) yielded higher bulk-velocity trends compared to the present study. These 2017 and 2018 studies were interpreted as evidence of rebounding stress-field conditions after a localized collapse between the 2014 (Figure 18b) and 2015 (Figure 18c) studies. Similarly to 2017 and 2018, the bulk-velocity trend has continued increasing in 2019, which further indicates a stage of rebound stress conditions.

Line 11

Line 11 is oriented N-S and crosses wells 2A and 4B at stations 1124 and 1151, respectively (Figure 20**).** Fundamental-mode information was confidently picked throughout a majority of the line from 4.5-18 Hz, despite a dominant higher mode observed in data from northern stations (below station 1135). The fundamental mode and higher mode exhibited similar dispersive characteristics such that this higher mode could be interpreted as a second fundamental mode. The presence of two fundamental modes is often attributed to a transition from one geology to another, which in this case occurs at stations surrounding well 2A. This transitional zone can be attributed to rebounding stress conditions observed in this location during previous studies. Overall, the bulk-velocity trend observed in 2019 is generally consistent with the 2017 and 2018 results such that no areas of concern have been identified at this time. However, given observations of changing stress conditions surrounding well 2A in earlier years, continued monitoring is recommended. Maximum inverted depth was limited to 58 m in 2019, which is 15-20 m shallower than depths achieved in 2017 and 2018. Although low-frequency information was observed below 4.5 Hz, the resolution of fundamental trend was low. Therefore, dispersion curves were picked conservatively to maintain high-confidence in the reported shear-wave velocity profiles.

Line 12

Line 12 is oriented NW-SE and intersects wells 6B and 7B located approximately at stations 1238 and 1219.5, respectively (Figure 21). The upper 15 m has an average shear-wave velocity of 175 m/s, which is consistent with unconsolidated sediment for this area. Top of shale bedrock is indicated by the velocity gradient at 20 m depth. Low-frequency signal (<4 Hz) was limited throughout most of the imaged area which subsequently resulted in decreased depth of investigation compared to surveys acquired in previous years. In an effort to overcome these limited low frequencies while preserving the more coherent higher frequency content, a 102 m spread was combined with a 72 m spread for stations west of 1220. Despite these attempts, the fundamental-mode trend, the maximum depth of investigation was still limited to 45 m due to a lack of source signal. Except for 2018, the average depth of investigation ranged from 50-60 m, therefore the depth achieved in 2019 is not uncommon for line 12. Overall, the bulk-velocity structure in 2019 remained generally consistent with previously reported results. It is suggested,

however, that monitoring continue for that area surrounding well 7B with increased coverage of its eastern portion to better understand why longer wavelengths are more readily acquired in this area compared to the western portion of the line.

Line 13

Line 13 is oriented W-E and intersects wells 7A and 4A located approximately at stations 1328 and 1376.5 respectively (Figure 22). Shear-wave velocities decreased by approximately 75 m/s between 20-40 m depth for stations east of 1335; last year, stations 1317-1335, which surround well 7A, were noted for a similar decrease in velocity. In 2019, aliasing affected the lowest frequency band of the fundamental mode (<4.5-5 Hz) which interfered with dispersion-curve interpretation in this same frequency range. Even with a longer spread size than previous years, (96 m vs. 75-87 m), this low-frequency portion of the fundamental mode could not be finely resolved. As a result, the maximum depth achieved with surface-wave inversion was approximately 40 m for a majority of the imaged area. This shallower depth of investigation is more consistent with the 2015 results where the average depth of investigation was 45-50 m. The 2019 bulk-velocity trend is also generally consistent with the 2015 results.

During interpretation of the 2019 dataset, the previously reported 2018 2D Vs profile for line 13 (Figure 22c) was re-evaluated to more thoroughly investigate the velocity changes noted surrounding well 7A. It was determined that dispersion curve interpretation has been challenging in this area due to interference from source signal from a different azimuth than previously thought. The change in shear-wave velocity structure, and possibly change in shale competency noted in the 2018 report, is still evident surrounding well 7A, but the decrease in shear-wave velocity from 2017 to 2018 is slightly higher (15% vs. 12% reported in 2018). Additionally, the average shear-wave velocity decreased by 12% at stations consistent with the location of 4A in 2018 compared to the current 2019 study. Based on the 2015-2019 studies (Figure 22), the 2017 study exhibited an elevated bulk-velocity structure compared to 2015, 2018, and 2019. Overall, it is recommended that monitoring continue over these wells to further evaluate these varying conditions.

Line 14

Line 14 is oriented W-E and extends across wells 3B and 1B, which are approximately located at stations 1442 and 1423 respectively (Figure 23). The upper 15 m has a shear-wave velocity of approximately 175 m/s, which is consistent with unconsolidated materials. Fundamental-mode signal evolved from a discontinuous to coherent and high-amplitude trend from western (i.e. 1459-1436) to eastern stations (i.e. 1437-1413). In the western portion of line 14, higher-mode energy is observed between 5-8 Hz starting from station 1449 until 1436 when the fundamental-mode trend becomes more continuous. Despite these challenges, a shorter optimal spread was used for 2019 data processing and dispersion-curve interpretation was performed with high-confidence to produce the 2019 result (Figure 23c). Since inverted velocities were reported to be 14% higher in 2018 for line 14, source signal characteristics were re-evaluated and the updated 2018 shear-wave velocity profile is shown in Figure 23b. It was determined that offline source energy was incorporated into the 2018 data processing that led to an apparent velocity structure. The shear-wave velocity profile for 2018 was re-estimated and the bulk-velocity trend is generally consistent for surveys performed from 2017 to the present.

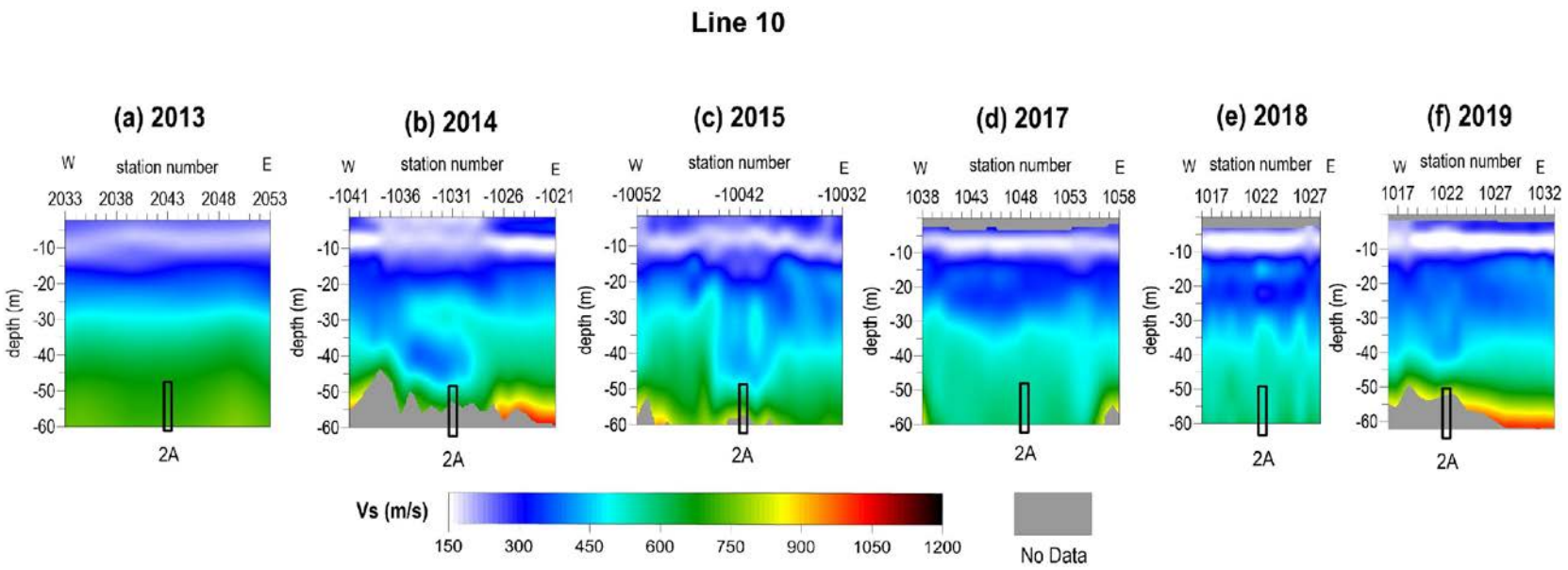

Figure 18. Shear-wave velocity profiles from line 10 from (a) March 2013, (b) November 2014, (c) Mary 2015, (d) November 2017, (e) October 2018, and (f) the current December 2019 investigation with approximate well locations.

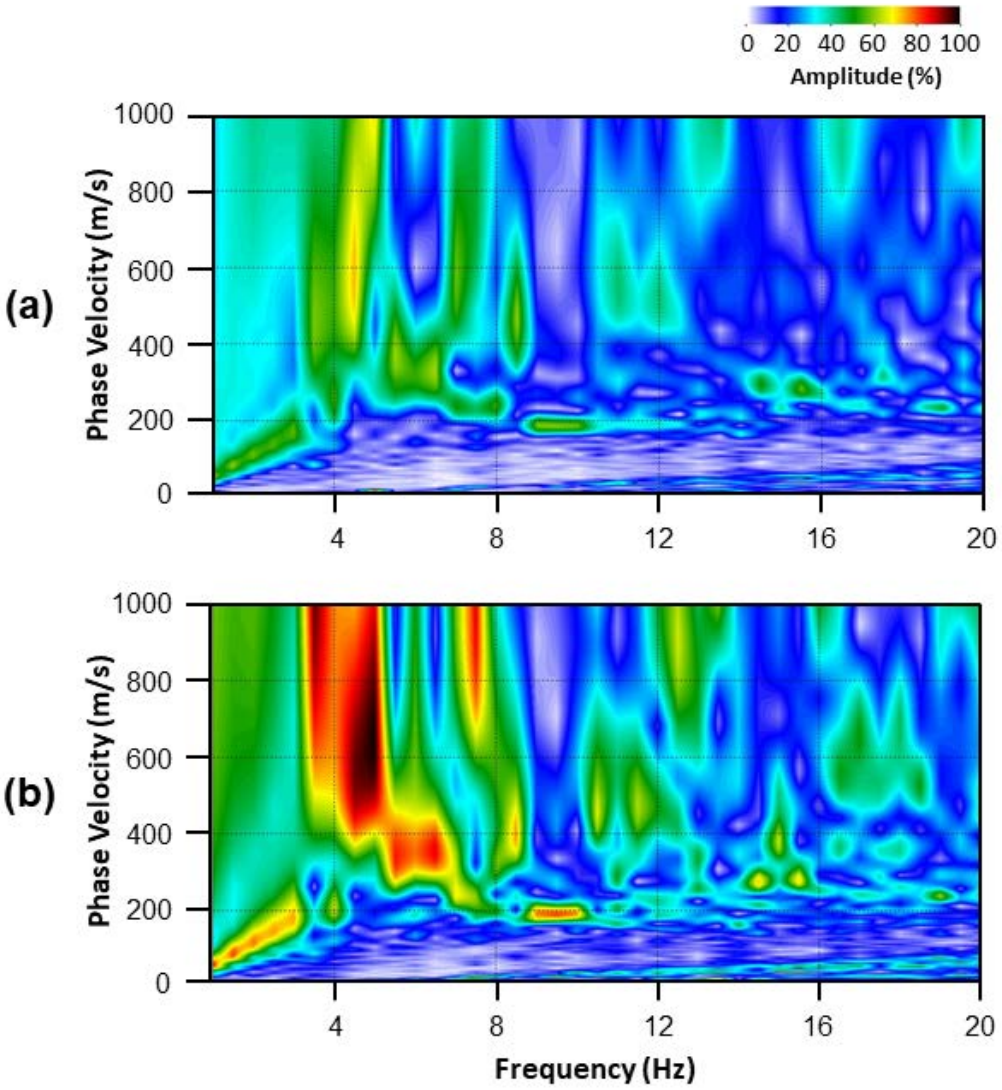

Figure 19. Example dispersion-curve images from line 10 where (a) western station 1017 exhibited increased signal attenuation compared to (b) station 1028 which exhibited a more continuous, high-amplitude fundamental-mode trend.

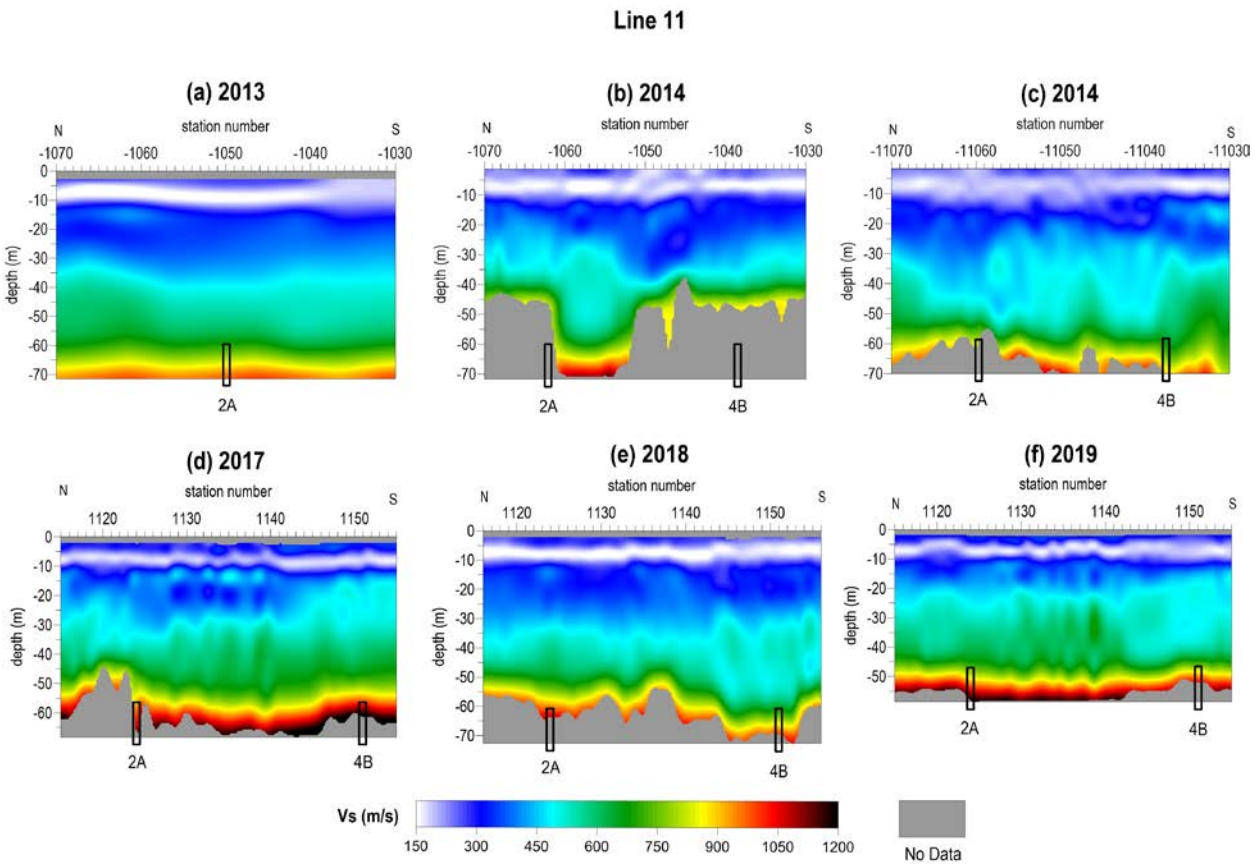

Figure 20. Shear-wave velocity profiles from line 11 from (a) March 2013, (b) November 2014, (c) May 2015, (d) November 2017, (e) October 2018, and (f) the current December 2019 investigation with approximate well locations.

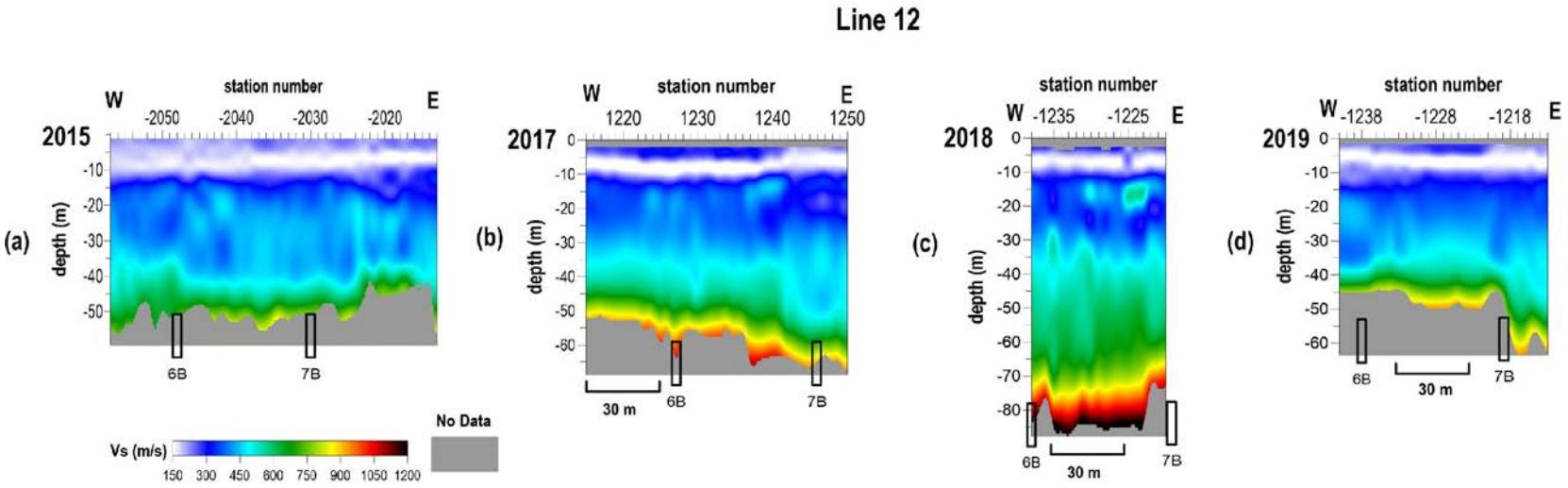

Figure 21. Shear-wave velocity profiles from line 12 from (a) March 2015, (b) November 2017, (c) December 2018, and (d) the current December 2019 investigation with approximate well locations.

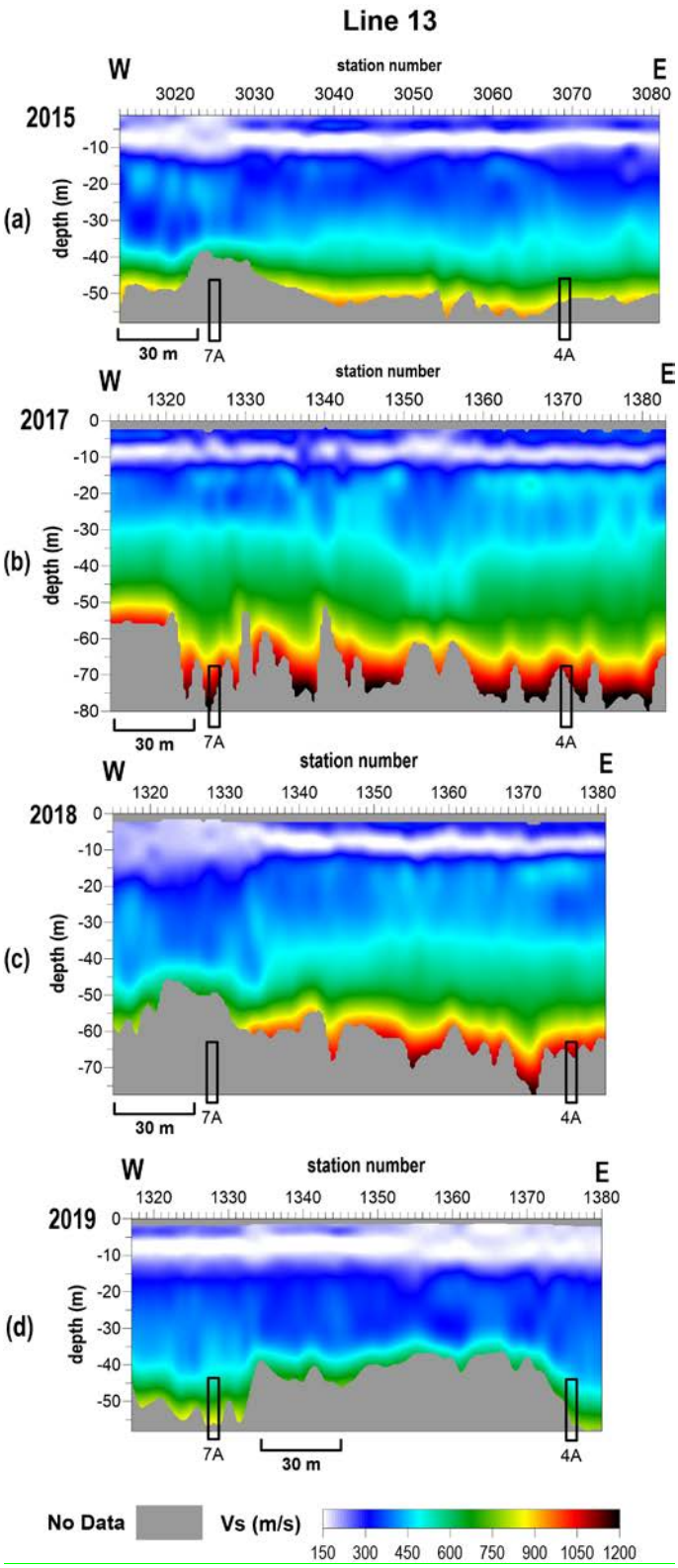

Figure 22. Shear-wave velocity profiles from line 13 from (a) March 2015, (b) November 2017, (c) December 2018, and (d) the current December 2019 investigation with approximate well locations.

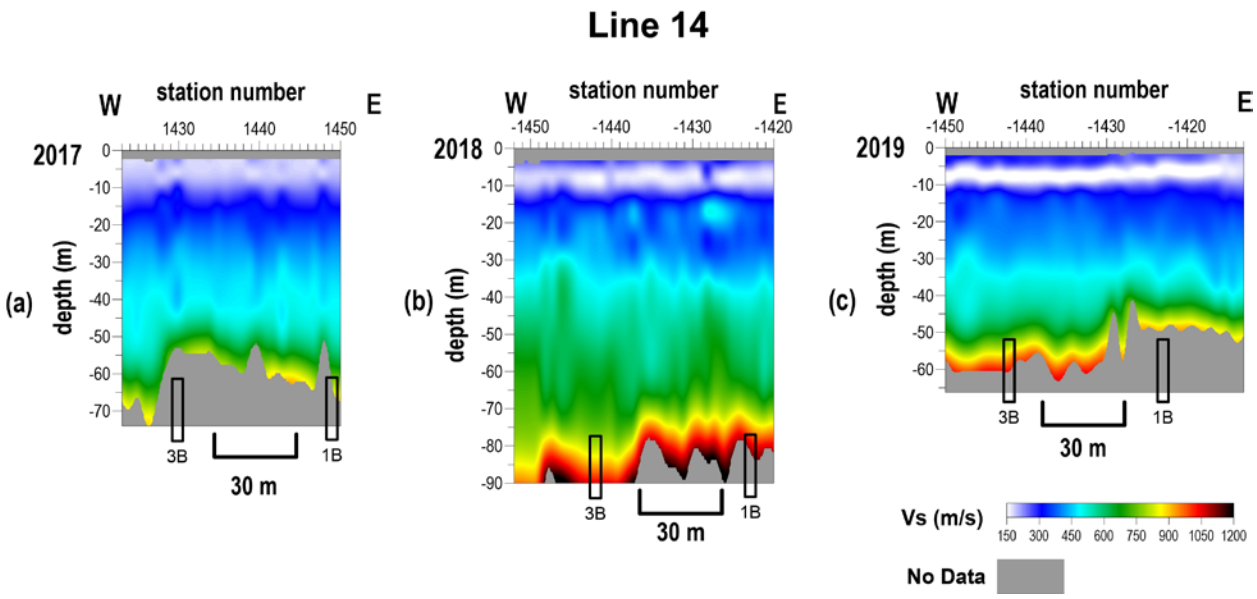

Figure 23. Shear-wave velocity profiles from line 14 from (a) November 2017, (b) December 2018, and (c) the current December 2019 investigation with approximate well locations.

Interpretation and Discussion

Wells with conditions of normal stress regime and consistent surface-wave behavior

Wells 4B, 13B, 18, 22A, 23B, 30, 39, 42, 46, 88, 89, 90

Wells with conditions of normal stress regime, but varied surface-wave behavior

Wells 2B, 8A, 10B, 11B, 17, 44, 45

Higher-mode surface waves dominated fundamental mode surface-wave energy on overtone images from stations in the proximity to these wells. This may be an indication of varying geologic structure in these areas, but the bulk-velocity trends surrounding these wells are consistent with previous surveys and likely represent a normal stress regime.

Wells 23B, 52, 53, 59, 60, 92

Increased depths of investigation were achieved on the 2019 survey in proximity to these wells compared to the 2018 study. Shear-wave velocity profiles acquired over these wells likely represent the natural geologic conditions with a normal stress regime.

Wells 17, 23, 29, 44

Surface wave signal was attenuated in proximity to these wells, but shear-wave velocity profiles acquired over these wells are consistent with previous surveys and likely represent the natural geologic conditions with a normal stress regime.

Wells 1B, 2B, 3B, 4A, 4B, 6B, 7A, 7B, 8B, 12B, 14B

Decreased depths of investigation were achieved in proximity to these wells compared to the 2018 study. Shear-wave velocity profiles acquired over these wells likely represent the natural geologic conditions with a normal stress regime.

Wells 41, 86, 87

Spreads cannot be extracted from these 2019 seismic lines with sufficient surficial coverage to extend directly over these wells for use in calculating the shear-wave velocity structure. However, the 2-D velocity structure of lines proximal to these wells do not possess anomalies consistent with apparent degradation in strength of material in proximity to these wells.

Wells with possibly varying stress regime

Well 2A

The 2019 results from lines 10 and 11 suggest that the shale bedrock is in a continued stage of rebound, similar to the 2017 and 2018 results. Two fundamental modes were observed below stations near the location of 2A, indicating a potential transition zone or zone of asymmetric stress conditions. Nonetheless, the bulk velocity surrounding well 2A is consistent with native material properties.

Well 7B

At this time, the bulk-velocity structure observed on line 12 in 2019 remained generally consistent with previous surveys and the measured velocities are in the range of

native material. However, the depth of investigation near well 7B was greatly reduced in 2019 with decreased velocity from 40-60 m; the depth of investigation was also reduced near well 6B, but the interpreted stress conditions and observed surface-wave behavior suggest a normal stress regime. To better evaluate this reduction in shear-wave velocity east of well 7B, additional monitoring with a longer array is recommended.

Wells 7A and 4A

In 2018, well 7A on line 13 was noted for a 12% decrease in bulk velocity and decrease in inverted depth since the 2017 survey. While the velocity trend near well 7A remained consistent, the bulk velocity near well 4A decreased by approximately 25% in the current study. Even with these reductions, the observed velocity ranges are still consistent with the native material. The maximum depth of investigation near well 4A decreased by 15 m compared to the 2018 survey at least in part due to reduced fundamental-mode velocity in the low-frequency range; the signal-to-noise ratio of the fundamental mode also suffered in the 2019 data. Interestingly, the 2019 bulk-velocity trend is consistent with the 2015 survey result; both 2015 and 2019 exhibited this bulk reduction in shear-wave velocity. Therefore 2017 and 2018 depict periods of slightly elevated velocity. Based on these observations, it is reasonable to suggest the shale bedrock may have experienced a decrease in material strength.

Well 15B

Since 2015, the area surrounding well 15B on line 7 has experienced changes in inverted depth and shear-wave velocity. Elevated velocity was first observed at 50 m depth in 2015, followed by periods of reduced velocity in 2017 and 2018. (Note: although elevated velocity was initially reported in 2018 near well 15B, re-processing of that dataset revealed that off-line signal was incorporated into the inversion result. Off-line signal, and the subsequent apparent velocity trend, were accounted for in the 2018 result reported in Figure 14c). While change in depth of investigation is not a direct indication of different shale competency/strength, the 10% decrease in shear-wave velocity adjacent to well 15B could be related to the shale stress conditions. In 2019, shear-wave velocity increased by 10% east of well 15B with an abrupt increase in inverted depth that was limited in the previous year. Due to a reduction in low-frequency signal at stations in the location of well 15B, it is unclear whether that increased velocity extends through that area. This incrementally increasing stress behavior in 2019 may represent elevated stress within the shale overburden. Given the high level of attenuated signal and change in velocity structure surrounding well 15B, it is challenging to make a more definitive interpretation without additional information from continued monitoring.

Well 59

Prior to the current survey, the stress conditions surrounding well 59 on line 9 were consistent with a normal stress regime. A slight increase in shear-wave velocity was observed near well 53 (directly north of well 59) between 40-60 m, but the interpreted surface-wave trends did not indicate significant change in the subsurface conditions. However, an elevated velocity anomaly was observed below 50 m depth under a station range that includes the location of well 59. This elevated velocity is 30% higher than the 2018 findings. In this elevated velocity region, fundamental-mode signal was

attenuated and less coherent than signal observed in other sections of line 9. Reduced signal-to-noise ratio in the fundamental-mode trend was also apparent in the 2018 dataset, but the inverted velocities were reportedly lower than the current study. This abrupt change in shear-wave velocity near well 59 may be an indication of increased stress conditions and monitoring is strongly encouraged.

Conclusions

The shear-wave velocity directly over or in proximity to a majority of the wells in this 2019 study represents natural geologic conditions and a normal stress regime. Shear-wave velocity images from four different well groupings have anomalies sufficiently outside the normal range with associated error bars to justify an increased awareness and monitoring on future surveys. Strength characteristics deduced from shear-wave velocities derived from the passive MASW surveys around wells 2A (lines 10 and 11), 4A and 7A (line 13), 15B (line 7), and 59 (line 9) indicate change consistent with either increasing stress or recent stress release suggestive of a relaxed or degraded state. These five wells represent the most likely threat to ground stability in the survey area.

Two wells experienced a noteworthy increase in shear-wave velocity. A 30% velocity increase was observed on the southern half of line 9, centered at well 59. Although no anomalous velocity profiles have been recorded at this well previously, such a large and abrupt increase may represent elevated stress and is worthy of attention. Elevated velocity at well 15B (line 7), compared to the previous two years, may suggest elevated stress. Similarly elevated velocity was observed at this well in 2015, followed by a return to native bedrock velocity (equilibrium conditions) in 2017 and 2018. This suggests incremental failure may be continuing at this well. Continued monitoring is strongly encouraged to better understand the source of these observed changes and monitor for signs of incremental failure and void migration.

The bulk velocity across line 13, which intersects wells 4A and 7A, decreased by approximately 25% relative to the previous survey. In 2018, the area surrounding well 7A was identified as having reduced velocity and shallower depth of investigation as a result of decreased velocity, decreased coherency in low-frequency surface wave trends, and increased higher-mode signal (which may indicate complex or distorted geologic setting due to fractures or other discontinuities). Based on findings from previous surveys and observations in the current study, there may have been a reduction in bedrock stiffness at and between wells 4A and 7A. While this possibility is concerning, it should be noted that velocity at depth does not suggest that the void has migrated into the shale bedrock at either of these wells (within the sampled depth range) and, therefore, additional investigation is not required at this time. Continued monitoring is strongly encouraged to monitor for signs of rebound or additional incremental failure.

At the time of this study, the area surrounding well 2A, intersected by lines 10 and 11, exhibited a slight decrease in shear-wave velocity relative to the previous two years. The development of a possible collapse feature at depth was indirectly observed in 2014-2015 as increased stress in the shale roof (overburden) rock. In 2017, evidence of this feature, indicative of deeper collapse, was minimized and shear-wave velocities continued to increase (rebound) through the 2018 study compared to 2014–2015. This change in velocity observed over the last five years indicates a buildup in stress (increased velocity) has been relieved (drop in velocity) and the bedrock material strength is returning to equilibrium conditions (velocity approaching surrounding rock) and near native bedrock velocities. In the present study, quality of the

fundamental-mode signal diminished in proximity to well 2A, where a decrease in both maximum depth of investigation and bulk velocity also occur. A transition in fundamental mode characteristics and quality may suggest asymmetric stress conditions. Nonetheless, the bulk velocity around well 2A is consistent with native material properties and likely represents relative stability at present following the previous period of rebound.

Recommendations

Seismic surveys at the CBRA over the last 15 plus years have provided insights and resolved some critical questions related to ground stability and the vertical migration of voids remaining from legacy salt solution mining that began almost a century ago. Clearly, passive surveying in this area is the most cost-effective way to confidently monitor change in the upper 70–80 m potentially related to vertical migration of voids toward the ground surface. Five areas associated with locations of legacy solution wells have been identified by the 2019 survey with characteristics that justify continued monitoring with focused analysis on future data sets. Wells 2A, 4A, 7A, 15B, and 59 have been identified on these data as possessing characteristics inconsistent with "native" shear-wave velocity measurements or with calculated shear velocities different from years past. New this year is well 4A and 59, dropping off last year's watch list is 89/90.

To that end, a reasonable path forward around well 2A would be **continuation of annual monitoring until stability in shear strength is observed on at least three consecutive surveys**, at which time the monitoring cycle can be reduced to every other year and potentially less frequently if stability appears consistent. This path forward allows for a current and reasonable understanding of subsidence risk around well 2A and for review after each survey for considering failure mechanics and associated subsidence potential and threat to surface structures or activity or groundwater in proximity to well 2A. Monitoring of this type and frequency would provide an early warning, by identifying changes in strength that might increase the chance for sinkhole development in advance of a breech in the bedrock surface and well in advance of any surface expression. If monitoring indicates a change is occurring in the subsurface, with the potential that a void has migrated above the 3-finger dolomite, then a complete review of previous surveys observed subsurface change and historical data can be used to determine whether additional investigation is warranted to directly appraise the void status. Consistent changes have been observed in each of the last three years (2017, 2018, and 2019).

With the 25% reduction in the bulk velocity near well 4A on the 2019 survey it is reasonable to suggest there has been a roof failure over the last year. Interestingly, the 2019 bulk-velocity trend is consistent with the 2015 survey result; both 2015 and 2019 exhibited this bulk reduction in shear-wave velocity. Therefore 2017 and 2018 depict periods of slightly elevated velocity. Based on these observations, it is reasonable to suggest the shale overburden has experienced a rupture near the top of the void roof. **Rock over this well needs to be monitored to determine if this was a unique event or part of a pattern that could be defining vertical migration of the void.**

The reduction in shear-wave velocity observed at well 7A in 2018 could have been an indicator of incremental roof rock failure at depth after the 2017 survey. Meaning a tensional dome above the abandoned mine void with a horizontal span that exceed rock strength could have failed and spalled, thereby relieving the overpressure, forming a new shallower roof with enhanced arch, and reducing the overburden stress/shear velocity. The velocity trend in 2019 is

consistent with 2018, suggesting the observed decrease in velocity is real and stress has returned (likely through incremental roof failure between the 2017 and 2018 surveys) to 2015 survey levels. Cycling in velocity from 2015 to 2018 is likely due to changes in the void's roof geometry through incremental collapse. The roof isn't necessarily stable, but deformation within the current roof span is in the elastic part of the stress/strain curve, hence a constant velocity. **It would be prudent to continue monitoring this area** for increases in shear velocity consistent with the 2016 and 2017 velocity levels. It is not clear if the stress increase observed in 2016 and released between 2017 and 2018, is a unique event or if this event is part of a cycle that has been experienced previously. Considering the proximity of 7A to the north property boundary **it will be important to appraise any changes observed over the next few surveys**.

Similarities in subsurface shear wave velocity change patterns in proximity of wells 4A and 7A, in conjunction with their location relative to the north property line, **justify continuing annual monitoring along line 13**. Currently both wells are experiencing relatively lower velocities and therefore lower states of stress with less potential to experience a roof failure. However, if the velocity cycle observed between 2015 and 2019 begins again, there might be reason to reevaluate the monitoring frequency of line 13.

The shear-wave velocity above well 15B increased this year, after two years of declines. This increasing stress following at least two years of decreases, increases the likelihood of some degree of incremental failure and vertical migration of the void toward the ground surface might occur. Considering the depth to the elevated shear velocity in the rock volume above the salt/shale contact it is reasonable to suggest void migration is likely, but with more than 40 m of relatively unstressed rock below the top of bedrock, it is very unlikely the void would reach the top of bedrock following a roof failure at this time. Considering the location of well 15B relative to the property lines, there are no threats to off-site structures. **Continued monitoring around well 15B would be prudent until measured shear wave velocities remain stable/consistent for at least three years**.

A decrease in bulk shear velocity observed during the 2018 has returned the area to a more normal velocity that is consistent with surveys prior to 2018. This observation reaffirms the suggestion that last year's dramatic drop in shear-wave velocity between wells 89 and 90 could have been the shear wave remnants of a gallery collapse. The migration pattern and timing is unknown and the event captured by the 2018 survey could be the first and only collapse with breccia halting continued vertical movement. With just a single year of decreased velocity it is difficult to determine the value of follow up surveys, but **this would be an area worth reviewing if future surveys are completed over these wells**.

Shear wave velocity calculated from the 2019 at well 59 was 30% higher than 2018. A velocity change of this order is significant, but the recommended next step depends on the well location relative to property lines and depth to top of high gradient velocity contours that marks to shallowest extent of the tensional dome. For well 59 there is still 20 m to the top of bedrock and the property line is well outside the angle of draw for this void. Therefore, another couple years of monitoring would be the logical next steps for well 59.

Over the past several years, wells in proximity to the property boundaries and with potential angle of draw extending outside the property boundaries have been the highest priority areas for investigation and analysis. Of particular recent interest has been the subsurface volume around well 2A, primarily due to the proximity of the Irsik & Doll elevator and the changes in stress interpreted to be originating from a volume approximately centered on well 2A. Changes measured at well 7A the last two years and now 4A this year, elevate the interest and dynamics

of the volume around the well in large part due to its proximity to the north property boundary. We propose a follow-up survey at these wells to ideally be completed annually (October/ November/December) with preliminary analysis of the area around wells 2A, 4A, and 7A completed before or near the end of the calendar year so results of the analysis can be provided to KDHE during early 2021. This would represent a good measure for evaluating stability and establishing a basis if any additional investigation at wells 2A, 4A, or 7A were needed for direct confirmation of void status.

At this point, a great deal of knowledge and understanding of the subsurface conditions around all the higher risk wells has been accumulated over the last several years. Since at least 4 of the 12 lines are recommended for additional surveys, and with some of the new discoveries unique to 2019 data, it seems reasonable to acquire another complete survey in 2020. The 2020 survey proposed here for the October/November/December time frame would include the entire CBRA with deployments near identical to 2019 allowing optimal coverage at all noted wells. An overall site analysis and report would be available during the spring of 2021.

References

Davies, W. E., 1951, Mechanics of Cavern Breakdown. Bulletin of the National Speleological Society, no. 13, 36-43.

Dellwig, L.F., 1963, Environment and mechanics of deposition of the Permian Hutchinson Salt Member of the Wellington shale: Symposium on Salt, Northern Ohio Geological Society, p. 74-85.

Dvorkin, J., A. Nur, and C. Chaika, 1996, Stress sensitivity of sandstones: *Geophysics*, v. 61, p. 444-455.

Eberhart-Phillips, D., D.-H. Han, and M.D. Zoback, 1989, Empirical relationships among seismic velocity, effective pressure, porosity, and clay content in sandstone: *Geophysics*, v. 54, p. 82-89.

Holdoway, K.A., 1978, Deposition of evaporites and red beds of the Nippewalla Group, Permian, western Kansas: Kansas Geological Survey Bulletin 215.

Ivanov, J., R.D. Miller, S.L. Peterie, J.T. Schwenk, J.J. Nolan, B. Bennett, B. Wedel, J. Anderson, J. Chandler, and S. Green, 2013, Enhanced passive seismic characterization of high priority salt jugs in Hutchinson, Kansas: Preliminary report to Burns & McDonnell Engineering Company.

Khaksar, A., C.M. Griffiths, and C. McCann, 1999, Compressional- and shear-wave velocities as a function of confining stress in dry sandstones: *Geophysical Prospecting*, v. 47, p. 487-508.

Kulstad, R.O., 1959, Thickness and salt percentage of the Hutchinson salt; *in* Symposium on Geophysics in Kansas: Kansas Geological Survey Bulletin 137, p. 241-247.

McGuire, D., and B. Miller, 1989, The utility of single-point seismic data; *in* Geophysics in Kansas, D.W. Steeples, ed.: Kansas Geological Survey Bulletin 226, p. 1-8.

Merriam, D.F., 1963, The Geologic History of Kansas: Kansas Geological Survey Bulletin 162, 317 p.

Merriam, D.F., and C.J. Mann, 1957, Sinkholes and related geologic features in Kansas: *Transactions of the Kansas Academy of Science*, v. 60, p. 207-243.

Miller, R.D., 2011, Progress report: 3-D passive surface-wave investigation of solution mining voids in Hutchinson, Kansas: Interim report to Burns & McDonnell Engineering Company, January, 9 p.

Miller, R.D., J. Ivanov, S.D. Sloan, S.L. Walters, B. Leitner, A. Rech, B.A. Wedel, A.R. Wedel, J.M. Anderson, O.M. Metheny, and J.C. Schwarzer, 2009, Shear-wave study above Vigindustries, Inc. legacy salt jugs in Hutchinson, Kansas: Kansas Geological Survey Open-file Report 2009-3.

Park, C., R. Miller, D. Laflen, N. Cabrillo, J. Ivanov, B. Bennett, and R. Huggins, 2004, Imaging dispersion curves of passive surface waves [Exp. Abs.]: Annual Meeting of the Soc. of Expl. Geophys., Denver, Colorado, October 10-15, p. 1357-1360.

Sayers, C.M., 2004, Monitoring production-induced stress changes using seismic waves [Exp. Abs.]: Annual Meeting of the Soc. of Expl. Geophys., Denver, Colorado, October 10-15, p. 2287-2290.

Sloan, S.D., S.L. Peterie, J. Ivanov, R.D. Miller, and J.R. McKenna, 2010, Void detection using near-surface seismic methods; *in* Advances in Near-Surface Seismology and Ground-Penetrating Radar, SEG Geophysical Developments Series No. 15, R.D. Miller, J.D. Bradford, and K. Holliger, eds.: Tulsa, Society of Exploration Geophysicists, p. 201-218.

Swineford, A., 1955, Petrography of upper Permian rocks in south-central Kansas: State Geological Survey of Kansas Bulletin 111, 179 p.

Terzaghi, K., 1936, Stress distribution in dry and in saturated sand above a yielding trap-door. In *Proc. 1st International Conference on Soil Mechanics and Foundation Engineering*, 307-311. Cambridge, MA: Harvard University.

Walters, R.F., 1978, Land subsidence in central Kansas related to salt dissolution: Kansas Geological Survey Bulletin 214, 82 p.

Whittemore, D.O., 1990, Geochemical identification of saltwater contamination at the Siefkes subsidence site: Report for the Kansas Corporation Commission.

Whittemore, D.O., 1989, Geochemical characterization of saltwater contamination in the Macksville sink and adjacent aquifer: Kansas Geological Survey Open-file Report 89-35.